Exploring mechanisms for bacterial width change using coarse-grained simulations of the peptidoglycan cell wall

A thesis
Submitted towards the partial fullfilment of
BS-MS dual degree programme
by

Ryth Dasgupta

Date: March 26, 2025

under the guidance of

Dr Sven van Teeffelen
Université de Montréal
from May 2024 to Mar 2025

Indian Institute of Science Education and Research Pune

Certificate

This is to certify that this dissertation entitled "Exploring mechanisms for bacterial thinning using coarse-grained simulations of the peptidoglycan cell wall" submitted towards the partial fulfillment of the BS-MS degree at the Indian Institute of Science Education and Research, Pune represents original research carried out by Ryth Dasgupta at Université de Montréal, under the supervision of Dr. Sven van Teeffelen during academic year May 2024 to March 2025.

Supervisor:
DR. SVEN VAN TEEFFELEN
ASSOCIATE PROFESSOR
UNIVERSITÉ DE MONTRÉAL

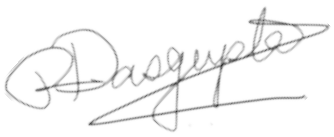

RYTH DASGUPTA
ROLL NO.: 20201062
BS-MS
IISER PUNE

DATE: MAY 15, 2025

Declaration

I, hereby declare that the matter embodied in the report titled "Exploring mechanisms for bacterial thinning using coarse-grained simulations of the peptidoglycan cell wall" is the results of the investigations carried out by me at the Université de Montréal from the period 14-05-2025 to 27-03-2025 under the supervision of Dr. Sven van Teeffelen and the same has not been submitted elsewhere for any other degree. (If multiple supervisors were involved, please separately mention what period the work was carried out under each of their respective supervisions, or whether it was concurrently co-supervised.).

Supervisor:
DR. SVEN VAN TEEFFELEN
ASSOCIATE PROFESSOR
UNIVERSITÉ DE MONTRÉAL

RYTH DASGUPTA
ROLL NO.: 20201062
BS-MS
IISER PUNE

DATE: MAY 15, 2025

Acknowledgements

I would like to thank my supervisor Dr. van Teeffelen for his invaluable guidance through to project. I am also indebted to the lab members of the van Teeffelen lab, and friends from the department of microbiology immunology and infectiology at the University of Montreal for their help and company through the project. Thank Finally, I thank my friends and family for their constant support.

Contributions

Contributor name	Contributor role	Role definition
Sven van Teeffelen	Supervisor	Ideation of research and guidance
Chaitanya Athale	Thesis Expert	Evaluation and guidance
Ryth Dasgupta	Researcher	Research, writing and presentation

Software used

This research was enabled in part by the support provided by:

- Mathworks MATLAB [24]: Data analysis, plotting
- Morphometrics [37]: Image analysis from microscopy data
- ImageJ (Fiji) [30]: Image analysis rendering
- Ovito [32]: Visualisation of simulations
- Calcul Québec and the Digital Research Alliance of Canada.

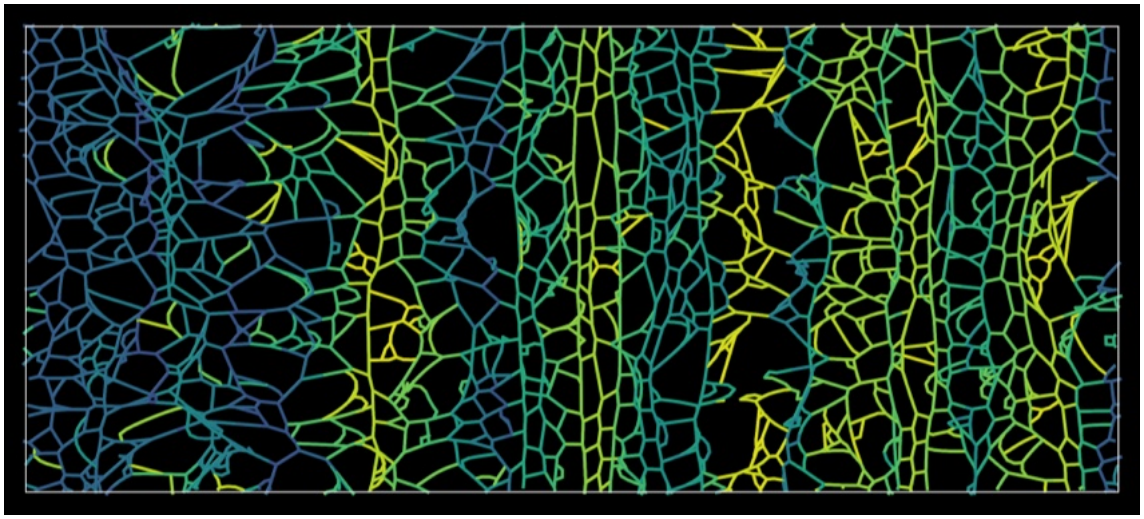

Figure 1: A coarse-grained simulation of the peptidoglycan cell wall

Abstract

Rod-like bacteria control cell width with high precision during growth. For a given species and growth medium, the variation in cell widths in a population is only about 5%. At the same time, the widths appear flexible when the cells are subjected environmental perturbations by changing their cell widths into a new steady state quickly. Despite decades of research on cell shape, how cells display such precise width control while also showing pliancy upon environmental perturbations remains unknown. Previous experiments have shown that the peptidoglycan (PG) cell wall is the major contributor to resisting the high intracellular pressures in the cell by forming a rigid scaffold around the cell. During growth, new PG is inserted into the cell wall and old material is broken down. Together, these processes result in the dynamic equilibrium that determines cell shape. To understand the effects of cell wall remodelling and PG topology on width homeostasis, we conducted coarse-grained computational simulations that mimic the cell wall and the processes of PG synthesis and breakdown. Different from previous simulations of whole-cell sacculi, we restrict our simulation to a small periodic patch of PG with dynamic boundaries that mimic the high intracellular turgor pressure. This allows for fast computation and thus for the systematic investigation of model parameters, e.g., the rates of cutting and insertion. Our computational simulations then allow us to systematically test different mechanisms of PG insertion and breakdown for their ability to decrease or increase cell width over time. We show that insertions of long, unstretched glycan strands when coupled with cutting of nearby PG bonds is sufficient to constrict the width of the cell over many generations, and the inhibition of such insertions results in an increase in cell widths.

Contents

Chapter 1

Introduction

Bacteria show an exceptional diversity in shapes. The examples shown in Figure 1.1 barely capture the full range of forms found in microbiology. Yet, it is fascinating that each bacterial species maintains its shape with remarkable consistency. In fact, the morphology for a given species is so reproducible, that it has been used to identify bacteria for decades [5].

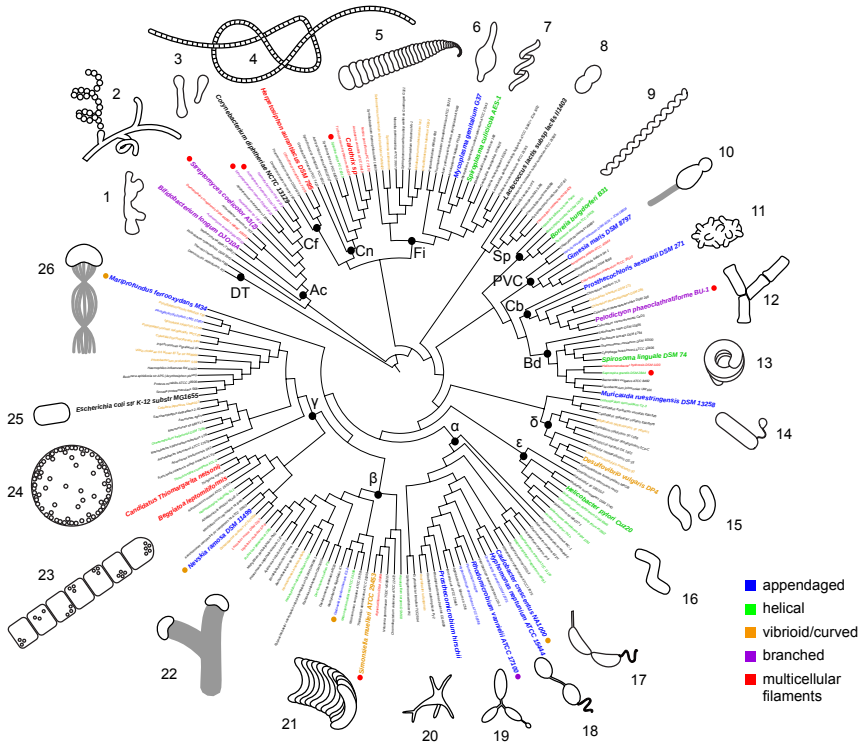

Figure 1.1: Immense diversity of bacterial morphologies, Figure 1 from Kysela et al. [23].

Rod-shaped, gram-negative bacteria are especially known for their tightly controlled shape. When grown in a given medium, their widths vary by only about 5% [46] across the population. This might make it seem that their shape is rigid; where they

elongate, without changing their width. However, bacteria can rapidly adjust their width in response to environmental or drug induced perturbations. For example, *Escherichia coli* cells growing in rich media are wider than those growing in poor media. When shifted from the rich to the poor medium, the cells plastically reduce their widths to reach the new steady state [27] and similarly, when shifted from a poor to a rich medium, they plastically increase their widths to return to their wider morphology.

Recent research has shed some light on how bacterial lengths are regulated [46]. However, the mechanism of width control - how cells orchestrate the fast and tight control over their diameter remains unclear. In this thesis, I focus on understanding how bacteria regulate their width. Specifically, I am interested in understanding the enzymatic processes that allow rod-shaped bacteria to rapidly increase and reduce their diameters.

1.1 The envelope remodelling system

To understand how cells control their shape, we must consider how they achieve any shape in the first place. It has been shown that the peptidoglycan (PG) cell wall confer shape to bacteria [43]. It does this by forming a rigid scaffold around the cells which resists the high intracellular turgor pressure while instantiating cell shape [6] [9] [20].

The peptidoglycan (PG) layer is part of the cell envelope. In Gram-negative bacteria, it is 2-4 nm thick and located between the inner and outer membranes [13]. Conversely, in gram positive bacteria, the cell envelop does not have the outer membrane, but has a much thicker and multi-layered PG layer. The PG layer consists of long, circumferentially oriented polymers of alternating N-acetylglucosamine (GlcNAc) and N-acetylmuramic acid (MurNAc) sugars, called glycan strands. Each disaccharide, also referred to as a glycan subunit, has a peptide stem attached perpendicularly, oriented helically around the glycan strand such that every other peptide is in the same plane as the PG layer. Adjacent peptides covalently link to each other, forming peptide cross-links that join glycan strands to each other to form a large covalent macromolecular mesh around the cell (Figure 1.2).

On average, glycan strands are 25 subunits long [13], but their length distribution has a long tail, with some strands reaching up to 200 subunits [36]. Depending on the enzyme that makes cross-links between the peptide oligomer stems on the glycan subunits, there are two types of peptide bonds: 4->3 peptide bonds, which link the 4th peptide (D-ala in *E.coli*) in the donor stem to the 3rd peptide in the receiver peptide stem (DAP in *E.coli*) as shown in Figure 1.2, and the 3->3 peptide bonds, which link the 3rd peptide in the donor stem to the 3rd peptide in the receiver.

Since the PG layer is a single rigid macromolecule, the only way for cells to grow beyond what stretching the covalent bonds can allow, is by enzymatically remodelling the cell wall. This involves cutting bonds and incorporating new material into the cell wall. This is called 'plastic' growth, since the enzymatic remodelling is

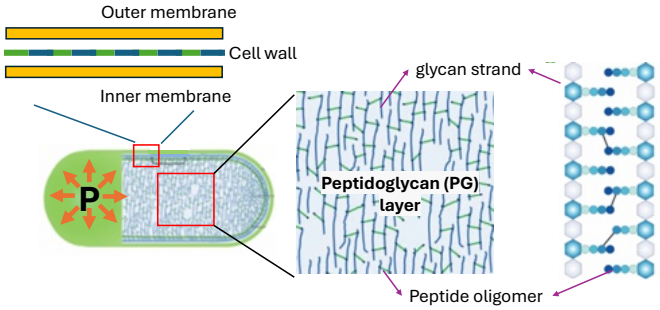

Figure 1.2: The peptidoglycan cell wall is a single, covalently linked macromolecule. Adapted from [13]. Blue hexagons: MurNAc; Grey hexagons: GlcNAc. P: intracellular turgor pressure.

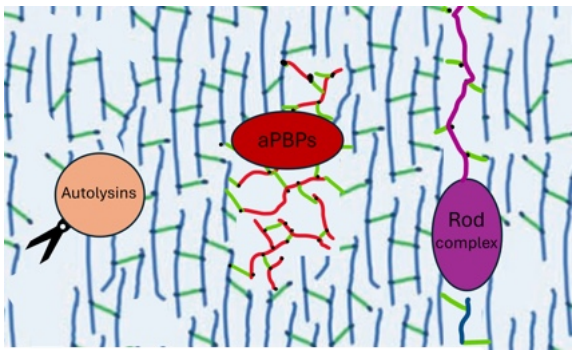

Figure 1.3: Enzymatic remodelling of the cell wall is essential for growth. The three main types of PG remodelling are cutting done by autolysins, repair done by aPBPs and insertion done by the rod-complex.

irreversible. In order to understand how this remodelling regulates width, it is important to understand the types of remodelling processes available to the cell.

Breakdown

In order to facilitate the incorporation of new PG material into the PG network, the old peptide and glycan bonds need to be cleaved. The peptide cross-links and glycan strands are cut by endopeptidases (EPs) and lytic transglycosylases (LTs) respectively. Together, they are called autolysins (Figure 1.3A). Autolysins, aptly named after their ability to cause cell lysis, reduce the structural integrity of the cells, and thus cells must regulate their activity very tightly. Unchecked autolysis can cleave too many bonds and lead to rupture. This is demonstrated by the overexpression of hydolases causing cell lysis seen both in the rod-shaped bacterium *B. subtilis* [31], and our own experiments with *E. coli* in section 4.2.

Bacterial autolysins form a large and diverse group of enzymes, with the ability to cleave every amide and glycoside linkage in the PG layer [44], although not every specificity is found in every species. Despite the diversity in the number of autolysins and their substrates, autolysins show remarkable redundancy. For example, *E.coli* endopeptidases MepM, MepS and MepH are redundantly essential, while all showing

very subtly different activities [13]. In fact, seven out of eight EP encoding genes can be deleted in *E.coli* while maintaining cell viability [42]. Another striking example of the flexibility of the autolytic system in maintaining cell viability is that cells can grow with all DD-EPs (EPs that cleave 4->3 peptides) deleted if the cells are grown in conditions where only the 3->3 peptide cross-links form [21].

With so many redundancies in autolytic activity, it is often difficult to understand the unique role of individual enzymes. For example, *E.coli* has multiple DD-EPs, LD-EPs, LTs and a number of other autolysins, all of which appear to contribute to growth and cell shape maintenance, and often show interchangeable functions. Thus, the regulation and specific role of distinct autolysins is still an open question in the field. Although the substrates for the autolysins are well characterised [13], *when and where* in the PG layer the enzymes cleave their respective bonds is not fully understood yet.

Regulation of the autolytic activity could be at the substrate, enzyme and transcriptional levels. For instance, autolytic activity could deplete its own substrate or the substrate of other enzymes, which might provide a robust feedback loop to control cleavage sites. One candidate for such a loop is age-dependent autolytic activity. Newly synthesized glycan strands have peptapeptide stems. The eventual activity of carboxypeptidases, another type of hydrolase EPs, cleave the last peptide from the oligomer to make it a tetrapeptide. As such, the activity of carboxypeptidases might increase the availability of substrates for a hydrolase that prefers cleaving cross-links made with tetrapeptide stems. For regulation the enzyme level, it has been shown that ShyA, an EP native to *V. cholerae* and MepM undergo conformational changes from 'active' to 'inactive' states and vice versa [31]. What mediates shift between the states is not fully understood. Protein-protein interactions are another way hydrolysis is regulated. In *E.coli*, the outer-membrane bound regulator NlpI associates with Prc protease to tightly control the abundance of MepS hydrolases [3].

Another regulatory mechanism for 'smart' autolysins proposed in 1990 by Koch is their dependence on mechanical stress in the system [22], as demonstrated by cells that respond to external bending forces by growing into curved shapes independent of cell wall insertion [21].

Synthesis

There are two types of synthesis of the PG layer: 1. Rod-complex mediated synthesis and 2. Class A penicillin binding proteins (aPBPs) mediated synthesis. , while the aPBPs are responsible for maintaining cell wall integrity [41].

The rod complex

The rod complex maintains the rod shape of the cell [40]. It is a large protein complex at its core comprised of MreB, MreC, MreD, RodA, RodZ and PBP2 proteins. RodZ coordinates with actin-like cytoplasmic filaments of MreB to insert long glycan strands into the cell wall [39]. RodA contains a transglycosylase (TGase) domain, which polymerizes glycan subunits into long glycan strands, and associates with

PBP2, a transpeptidase (TPase) which cross-links adjacent glycan strands via peptide bonds. Additional peripheral proteins regulate its activity and mediate MreB binding and orientation [28].

MreB filaments have an intrinsic curvature that aligns them with the circumferential direction of the cell [17]. This, in turn, directs the rod-complex to align circumferentially and move along the MreB as it inserts long glycan strands in its wake. [38] [35]. It has been seen that inhibiting rod-complex mediated insertion causes cells to lose their rod shape and and become spherical [27], demonstrating that the insertion of long, circumferentially aligned glycan strands into the PG layer plays a vital role in rod-shape maintenance. Even for cells that have been forced to grow spherically, the Rod-complex is able to rescue cylindrical shape [6]. Recent experiments using florescent labelling of cell walls along with microscopy has shown that local cell walls elongations temporally and spatially co-localise with MreB persistence, implying that the activity of the rod-complex leads to local cell elongations along its length [38].

Repair

Class A penicillin-binding proteins (aPBPs) are inner membrane-bound enzymes that play a key role in maintaining the structural integrity of the bacterial cell wall. They are bifunctional, with an N-terminal transglycosylase (TGase) domain that polymerizes glycan strands and a C-terminal transpeptidase (TPase) domain that cross-links peptides in the peptidoglycan (PG) mesh [13]. While aPBPs do not contribute directly to the determination of cell shape, they are crucial for preventing the formation of large pores in the PG by inserting short glycan strands at discontinuities in the wall [41].

There are two main types of aPBPs in E. coli: PBP1a and PBP1b. Though functionally similar, they contribute to cell wall synthesis in different ways. PBP1a primarily operates along the lateral sides of the cell and works in coordination with the shape-determining synthase PBP2, suggesting a role in elongation. In contrast, PBP1b is found both along the sidewalls and at the division site, where it associates with division machinery and helps in septal PG synthesis [41].

The activity of aPBPs depends on outer membrane-anchored cofactors: LpoA activates PBP1a and LpoB activates PBP1b. These cofactors stimulate the TGase and TPase domains of their respective synthases and are essential for proper enzymatic function. Importantly, these aPBP–cofactor complexes are thought to detect and respond to local damage or gaps in the cell wall. Rather than being guided by cytoskeletal elements like MreB, aPBPs and their cofactors move diffusely along the membrane, scanning for sites where repair is needed.

This repair role is distinct from the directional cell wall synthesis carried out by the Rod complex. When acting independently, aPBPs can drive isotropic expansion of the cell envelope. In addition, they provide robustness under stress conditions. PBP1b, in particular, is involved in responding to PG damage and may function independently of the Rod system. Along with L,D-transpeptidases, which form

alternative cross-links resistant to beta-lactam antibiotics, aPBPs form an important part of the bacterial response to cell wall stress.

The question of width regulation

Given that cells can only grow and change shape through the enzymatic remodelling of the PG layer, it is unclear how enzymes on the nanometre scale coordinate to control a macroscopic quantity like cell diameter. Intuitively, cutting and adding material to the cell wall should both cause it to expand. How, then, are they able to constrict the cell diameters? Additionally, when small local defects in width appear in the cell, how are small bulges in width reduced while small constrictions increased within a single bacterial cell, maintaining a consistent width along the cell length (section 4.1)?

1.2 Standing on the shoulders of giants

To summarise from the preceding discussion, it is clear that 1. autolysis[1] is necessary for cell growth, 2. Rod-complex activity maintains rod-shape and 3. aPBP mediated PG repair is required for the integrity of the cell wall. The question is; how do these processes coordinate in time and space to give rise to width control?

Nano-scale imaging in live cells is very difficult for various reasons. For instance, high-powered lasers that are often required for fluorescence imaging can lead to phototoxicity in the cells, or molecular tags may have inadvertent effects on the function of the cells. Electron microscopy needs fixed samples, which makes it incompatible with live cell imaging [25], and atomic force microscopy (AFM) can be much too slow to measure dynamic changes in the cell [35]. Without nano-scale imaging, it is difficult to understand how proteins localize, when they act, or how their activity changes upon environmental perturbations.

An alternative is perturbation studies, where selective inhibition or activation of key enzymes, individually or in combination, can induce different cellular phenotypes. These phenotypes can help deduce the function of the modulated enzymes. While successful, such studies can sometimes be inconclusive, as different perturbations often result in identical morphologies. For example, inhibiting different parts of the rod complex, such as PBP2 and MreB, both lead to a loss of cell shape and rounding, making it difficult to distinguish their functions [34]. Constraining the number of possible hypotheses can guide experimental design and improve the interpretability of seemingly similar results. A good way to constrain hypotheses and decide what to test is to build computational models of the system and test various mechanisms *in-silico*.

There are a number of models in the literature that give unique insights into how cells regulate their widths. Notably there are those that treat the cell envelope as a fluid continuum model where the cell growth is driven by pressure [2] [20]. These types of models are useful in understanding the dynamics of cell shape over a longer temporal

[1] Cutting of peptide/glycan bonds

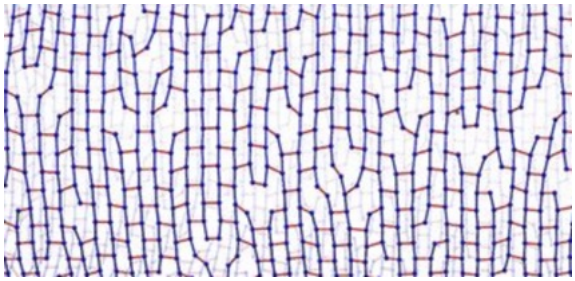

Figure 1.4: An illustration of the coarse-grained representation of the PG layer; glycan springs (blue) cross-linked to each other by peptide springs (red) at nodes. Figure from Nguyen et al. 2015, Figure 1D [26]

and spatial scales. They treat the cell wall as a fluid system, where the cutting and remodelling of the system is driven by the pressure. These models are useful in getting effective mechanical properties of the cell envelopes in various conditions, and also are much easier and faster to work with because they have only a few parameters. As such, continuum models might be preferred when quantifying the effective mechanical properties of cells during various drug or nutrient perturbations to understand what effect, say, MreB inhibition using A22 (drug) treatment has on the rigidity of the cell wall [20] [9] [33]. However, continuum models are not ideal to probe the mechanism of PG remodelling which leads to shape homeostasis, since the different remodelling systems change the system at scales much smaller than what the continuum models can probe.

To understand PG remodelling, it is more instructive to explicitly simulate the cell-wall and the various remodelling processes therein, using molecular dynamics (MD) simulations [16] [12] [15] [26]. MD is a computational technique that models the motion of atoms or molecules using Newton's laws of motion. It allows researchers to code in biomolecular interactions, structural dynamics, and conformational changes into their systems and watch its evolution in time.

Coarse-grained MD simulations are principally the same, but the atomic and molecular details are approximated into simple interactions, where multi-atomic molecules become a single 'node', and interactions between them are modelled using springs instead of physically accurate forces. In this case, coarse-grained MD simulations of the PG layer look like a network of many glycan and peptide 'springs', which are connected together at 'nodes', illustrated in Figure 1.4.

Although these models have many free parameters, are computationally expensive and slow to run, they offer a unique advantage of independent and specific control of every aspect of the system. Here, turning on and off different functions and forcing co-localisation of proteins to see how they behave is feasible, which makes mechanism exploration tractable.

Using coarse-grained MD similar to what is depicted in Figure 1.4, Furchtgott et al. simulated an entire cell wall sacculus along with a proposed mechanism for insertion, which demonstrated how cells might regulate their widths, keeping it constant over multiple doublings [12]. Here, they simulated insertion by the rod-

complex by weaving in the new glycan strands in between the old glycan strands; cutting peptide cross-links and making new ones as they went. To regulate width over many generations, this type of insertion needed to stretch the glycan strands by up to 10% before insertion, so that upon insertion the system did not expand. While their model showed a remarkable consistency in width over many generations, there is little evidence for any enzymatic process that could pre-stretch a glycan strand by such an amount. Glycan strands are stiff, and by some rough estimates [26], it would take of the order of 500 pN of force to stretch a strand by 10%, which is an exceptionally high force for enzymes to exert during insertion.

Nguyen et al. revisited the width homeostasis mechanism with a paper in 2015 [26]. This paper started with highly detailed atomic scale MD simulations of glycan strands and peptide stems. First, they showed that glycan strands are best represented as stiff linear springs, while peptides are best represented as worm-like chains (more details in section 2.1). Using this, they made a coarse-grained model for the entire cell sacculus. On top of simulating extremely detailed rules for each of the enzymes independently, they also tested multiple co-localisation and enzymatic coordination hypotheses. Their model was able to show width conservation without the need for pre-stretching over many generations, and proposed ways in which enzymes work together to achieve stable width control.

Both these groups pioneered the use of MD to probe the shape regulation in bacteria, and demonstrated how bacteria might keep a consistent width over multiple generations. However, the models do not show any width control: systematic increase or decrease of width. They maintain the widths that the simulations started with, but do not give clues into how cells might increase or reduce its width systemically depending on their growth conditions. The feedback loop for the cell to achieve a set-point width remains an open question. Additionally, owing to the size of these models, they were not able to explore a large parameter space, and only showed width conservation for a narrow range of conditions.

Because atomic scale MD simulations are extremely computationally expensive, it is not feasible to simulate the entire PG sacculus in atomic detail. The models by Furchtgott et al. and Nguyen et al. were able to circumvent this by simplifying the atomic detail into ball-spring interactions. However, Gumbart et al. [15] used a different way to make atomic-scale MD simulations of the PG layer tractable. Instead of simulating the entire PG sacculus, they simulated a small patch of the layer with periodic boundary conditions. Periodic boundary conditions are a way to simulate an infinite system by making the opposite edges of a simulation box connect. So, when a strand exits one side, it re-enters from the opposite side. This allowed Gumbart et al. to make a small system behave like a much larger one, thus being able to save on computational costs while still maintaining the large-scale order of the system. However, being an atomic scale model, it was still prohibitively slow to be able to iterature through many runs over long periods of time. While they were able to comment on the physical properties of the pg layer with their model like the stiffnesses or the distribution of holes, they did not simulate growth or remodelling.

Taking inspiration from Nguyen et al.'s coarse-grain structure and Gumbart et al's [15] periodic boundary conditions, we tried to address width control in our simulation by building a small, fast and detailed computational model of the PG layer, capable of growth (section 2). In this work, we propose a mechanism for persistent width decrease, and use our model to demonstrate it. We also perform some preliminary experiments in order to inform the model, and justify its validity despite its smaller size (section 3.6).

Chapter 2

Modelling the peptidoglycan cell wall: The 2DPG model

Cell widths are controlled by the PG layer, which in turn is constantly being reorganised by enzymes that cut and insert PG material. The three remodelling processes are autolytic cutting (section 1.1), rod-complex mediated glycan insertion (section 1.1) and aPBP mediated repair (section 1.1). It is not understood how these processes come together to give rise to width control, and a good way to begin answering such a question is to simulate the processes, and see how they interact to change system sizes.

The current models in the literature show width conservation rather than control. In other words, they show how widths can remain constant, but they do not explain how the cell might systematically increase or reduce its width into a new steady state depending on environmental perturbations. Additionally, recent work has shown that these processes are generally independent of each other [10] [41], which these models do not incorporate.

In this chapter, I describe the development of a new model that can help answer how the processes individually contribute to width regulation by implementing the remodelling processes as independent events.

Similar to Nguyen et al and Furchtgott et al., [16][26], we represent the PG layer as a network composed of nodes and bonds. One glycan bond corresponds to one glycan subunit (see section 1.1), and a peptide bond corresponds to a peptide cross-link. For each glycan subunit, one of the disaccharides has a peptide stem, which allows it to bond with adjacent peptide stems to make a peptide cross-link. Only about 50% of all peptides are in the same place as the PG layer, while the rest are jutting 90°to the layer, and are less likely to be involved in cross-linking adjacent glycan strands (Figure 2.1). The degree of cross-linking varies between species and even growth conditions within a single species [43]. For *E.coli*, about half of the peptides are linked and the rest are free [14]. Nodes[1] correspond to locations where bonds connect to each other.

[1] I often use 'node' interchangeably with 'particle'.

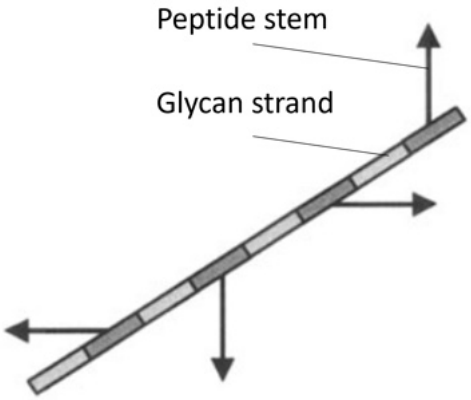

Figure 2.1: A cartoon representation of a glycan strand, where every peptide stem is 90°from the other forming a helical pattern. This results in the peptide pointing in the same direction every four glycan subunits, and half the peptides being in the same plane. Figure adapted from [43].

We simulate a small patch of the cell wall that is much smaller than the full sacculus width (500 nm) but larger than individual enzymes (5 nm). This reduces computational costs by limiting the model size and simplifies the system by treating the patch as a flat surface. Following [15], we apply periodic boundary conditions so that long glycan strands behave as continuous loops. The simulation box size determines internal stresses since a larger box spreads the nodes farther apart, increasing stress. To mimic the stresses of a cylindrical shell, we allow the box size to adjust dynamically until the stresses in the x and y directions match their target values based on the radius (2.6).

Detailed atomic scale molecular dynamics simulations by [15] concluded that glycan bonds behave like stiff linear springs, while peptide bonds are best modelled as worm-like chains. Using their force-extension curves respectively, at each time-step of the simulation, forces are calculated and positions of the nodes in the network are updated under the assumption of over-damped dynamics, until the system reaches equilibrium. The steps are detailed in the following section.

2.1 The physics of the peptidoglycan layer

Glycan bonds

Glycan bonds can be approximated by stiff linear springs, with a stretching stiffness $k_g = 5570\ pN/nm$, and a bending energy of $k_b = 83.6\ pNnm$. The stretching force on a node on the glycan strand is given by:

$$F = k_g \Delta x \tag{2.1}$$

where $\Delta x = l - l_g$ is the extension of the glycan bond away from its rest length $l_g = 1nm$.

The forces exerted on the nodes due to bending are derived from the energy equation:

$$E_b = \sum_{p_1}^{p_N} \frac{1}{2} k_b (\alpha)^2 \tag{2.2}$$

Where p_i is the index number of the nodes in the system, and α is the angle the bonds make at each node (Figure 3.9). By taking the negative gradient of the energy in terms of Cartesian coordinates at each particle, we find the equation of the force on that particle ($F = -\nabla_p E_b$):

$$\mathbf{F}_{p_2} = k_b \alpha \frac{\hat{\mathbf{b}} - \hat{\mathbf{a}}}{\sqrt{1 - p^2}} \tag{2.3}$$

Where $\hat{a}$ and $\hat{b}$ are the unit vectors joining nodes p_1 and p_2, and p_2 and p_3 respectively, and $p = \hat{a} \cdot \hat{b}$, α is the angle that the bonds make at node p_2. To make sure linear momentum remains zero for the system, we also equally distribute an opposite force on the p_1 and p_2 as shown in (2.4). This is an approximation of the real forces since it does not guarantee the conservation of angular momentum. Ideally, the opposite forces on p_1 and p_3 should be distributed based on the individual bond lengths $|a|$ and $|b|$. But, since the glycan strands are stiff and do not stretch more than 1-3%, it is a valid approximation that $|a| \approx |b|$.

$$\mathbf{F}_{p_1} = \mathbf{F}_{p_3} = -\frac{k_b \alpha}{2} \frac{\hat{\mathbf{b}} - \hat{\mathbf{a}}}{\sqrt{1 - p^2}} \tag{2.4}$$

Peptide bonds

From Nguyen et al.'s atomic scale MD simulations of peptides [26], we know that peptides are best represented as worm-like chains. The force-extension curves of the worm-like chain is given by equation (2.5).

$$F(x^*) = k_{\mathrm{WLC}} \left(\frac{L_c^*}{4(1 - x/L_c^*)^2} - \frac{L_c^*}{4} + x^* \right) \tag{2.5}$$

where $L_c^* = L_c - x_0$ is the effective contour length, L_c is the contour length, x_0 is the extension (end-to-end distance) x at which the force is 0, $x^* = x - x_0$ is the effective extension, and k_{WLC} is a force constant.

The values of the constants are taken from Nguyen et al. [26], tabulated in Table A.1.

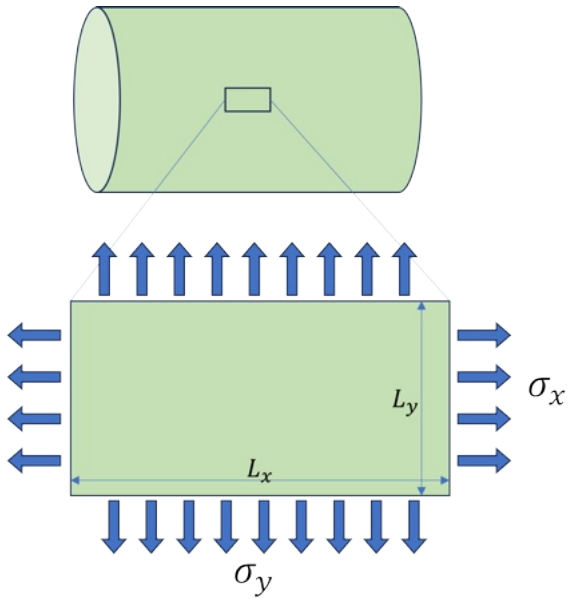

Figure 2.2: the 2DPG model simulated a small patch of the cylindrical part of the rod-shaped bacteria (green surface). The stresses (σ) defined as the force per unit length it's acting on, are shown by the blue arrows. This small patch is almost perfectly flat, making it feasible to use periodic boundaries.

Pressure

Since the PG layer holds the pressure of the cell, the stress on the PG layer is directly proportional to the turgor pressure. As a result, the internal turgor pressure is simulated by modulating the stress on the PG layer in the x and y direction to match those that are calculated for a cylindrical cell with a turgor pressure P. In a pressurised thin cylindrical shell, the 2 dimensional stresses in the x and y directions are anisotropic, and are given by equation (2.6):

$$\begin{aligned} \sigma_x &= Pr \\ \sigma_y &= \frac{Pr}{2} \end{aligned} \tag{2.6}$$

Where r is the radius of the cylinder, P is the pressure inside the cylinder, σ_x is the force per unit perpendicular length of the cylinder along the long-axis and σ_y is the force per unit perpendicular length of the cylinder along the circumferential direction as shown in Figure 2.2.

2.2 Simulation algorithms

MD position update

For each type of bond, we maintain a list of bonded node pairs. We iterate through this list and calculate the distance between the bonded pairs of particles, then use

the equations mentioned above to calculate the respective forces.

After all the forces are calculated, the positions are updated by looping over all nodes and adjusting their positions assuming an overdamped system, as described by:

$$\delta \mathbf{r} = \mu \cdot dt \cdot \mathbf{F} \tag{2.7}$$

where dt is the timestep value chosen empirically, μ is a coefficient of friction, and $\mathbf{F}$ is the net force on that node.

While updating positions, the step sizes $\delta \mathbf{r}$ are normalized such that the maximum step size is set to `max_stepsize` to avoid numerical instabilities and oscillations.

The positions are updated in a loop until one of two criteria are met: 1) The system reaches equilibrium, or 2) The maximum number of loop iterations (`timesteps`) is reached. Equilibrium is determined by the coefficient of variation of bond lengths. If the coefficient of variation of the bond lengths in the last 3,000 iterations changes by less than 0.05%, then the system stops updating positions and moves on to the next step. In most simulations, the maximum number of steps was set to 100,000. This number was empirically chosen after a few test runs showed it took around so many timesteps to reach equilibrium. The equilibration codes are written in C and compiled as a shared object module, which is then called into the Python script. This allows for much faster and parallel computations in C, while also maintaining the readability and modularity of Python for the more complex remodelling algorithms.

Simulating pressure by changing the boundary box size

To calculate the stress in the x direction, all bonds that cross the centerline at $x = 0$ are temporarily cut [2] The x components of the resultant forces on the left node of each bond-pair are then summed and divided by L_y, the system size in the y direction, as shown in equation (2.8). Here, n represents the relevant nodes on one side of the centerline, $\mathbf{F}_x$ is the force in the x direction, and L_y is the system size in the y direction.

Similarly, to calculate the stress in the y direction, the midline at $y = 0$ is considered. The sum of the forces along the y direction on the particles is then divided by L_x, the system size in the x direction, as shown in equation (2.9).

$$\sigma'_x = \sum_n \mathbf{F}_x / L_y \tag{2.8}$$

$$\sigma'_y = \sum_n \mathbf{F}_y / L_x \tag{2.9}$$

[2] Without updating their positions.

Once the stresses are determined, the size of the periodic boundaries are modulated by varying L_x and L_y:

$$\begin{aligned} \delta L_x &= (\sigma'_x - Pr/2) \cdot dt \\ \delta L_y &= (\sigma'_y - Pr) \cdot dt \end{aligned} \tag{2.10}$$

where δL_i is the step size by which we increase the boundary box dimension along i, σ'_i is the stress measured from the simulations, P is the internal pressure of the cell, r is the radius of the cell and dt is a simulation time-step (see Table A.1). Note here that for all simulations in this paper, the radius r is set to 400nm unless otherwise stated.

As while updating positions, we capped the step size (δL_x) to `max_box_step`. Finally, this results in the box reaching a size where the stress in the x and y directions match their set point values.

Simulating insertion of new glycan strands

The Rod complex inserts straight and long glycans that are circumferentially oriented [40], and forms cross-links with available peptide stems from adjacent strands, such that approximately half the peptides are bound [14] [15]. The orientation of the inserted glycans is independent of the local disorder of the PG layer or growth conditions, but the amount of cross-linking depends on environmental conditions. In exponential growth phase for *E.coli*, the degree of cross-linking is approximately 40-50% [14].

One proposed mechanism for the way the rod-complex works is the 'make-before-break' strategy of insertion [18]. At the scale of the enzymes, the rod complex aligns with the MreB, and its TGase domain polymerises a new glycan subunit into the growing glycan strand. The TPase domain presumably 'searches' for free peptides within a certain distance and cross-links available peptides to the newly inserted subunit. Finally, the stress-bearing bonds near the insertion are cleaved by hydrolases, which then pulls the newly inserted strand into the PG network due to the tension in the surface. This mechanism of insertion prevents the cells from lysing by making the new bonds before cutting older bonds under tension. By cutting the stress-bearing bonds near the inserted strand, it is ensured that the newly inserted strand is actually incorporated into the PG layer.

We model this strategy insertion using a simplified algorithm. We start by randomly placing an (infinitely) long, vertically (circumferentially) aligned glycan strand at a random x-location. The number of subunits in the newly inserted glycan strands is determined based on the current width of the system, such that it is the minimum number whose addition in a loop does not cause any constriction on its own. In other words, the number of added subunits n is given by $n = \texttt{ceil}(L_y/l_g)$; where L_y is the width of the system, and l_g is the rest length of the glycan subunits. The ceiling function ensures that the strand is never pre-stretched, although it might occasionally by pre-compressed due to this kind of rounding. Having placed an appropriately sized strand, we then test how many cross-links can be made by the

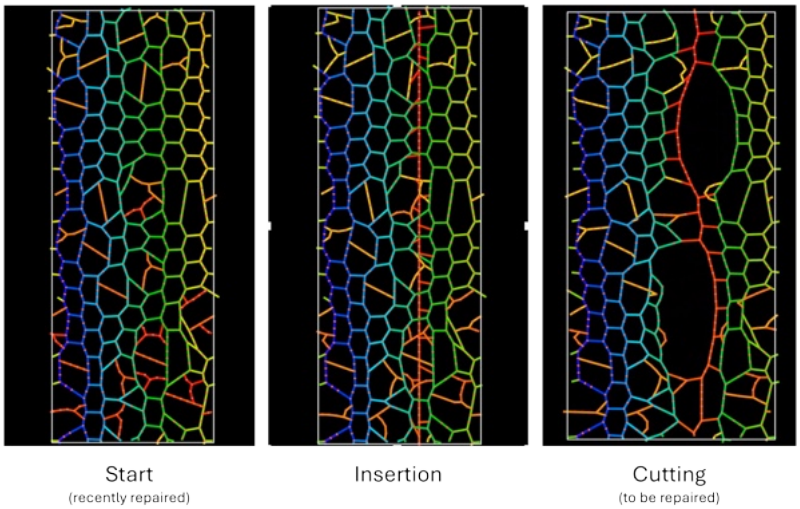

Figure 2.3: (Left to right) Initial system; A long, un-stretched glycan strand is inserted and cross-links are made with available nodes in the vicinity (red); The bonds that are crossing over are cut, and the system is allowed to relax. This leads to large pores, which need to be fixed.

nodes on the new glycan strand whose peptide stems are in the plane of the 2DPG layer. If the density of possible cross-links along the circumferential direction is greater than a pre-defined value `cl_min`, we randomly choose and make peptide cross-links until a density of `cl_max` is reached[3]. After making the new cross-links, all bonds that 'cross' the new glycan strand are cleaved, resulting in the older PG to separate and transfer the stress onto the new glycan strand. This is illustrated in Figure 2.3. For a detailed algorithm for insertion, please read section A.2. When we tried implementing insertion without the autolytic activity, we saw a constriction in cell length and glycans clumping together. This is discussed in a little more detail in the appendix (section A.3).

Simulating breakdown

Different from cutting the under-lying bonds during insertion in section 2.2, We also simulate the effect of autolysins independently of the rod-complex. Since not much is known about when and where autolytic activity occurs, we begin with the null-hypothesis of autolytic activity being random across the PG layer.

A pre-determined percentage of peptide and glycan bonds are randomly chosen and cut, as illustrated in Figure 2.4. As the system size grows, so does the number of bonds. In our simulations, these numbers will be denoted by `pcp` and `gcp`, which stand for peptide cut percentage and glycan cut percentage respectively.

Additionally, we added a `degrade` function, which identifies and removes bonds that are only connected to the network by one end, i.e. not carrying any tension. This cleans up the simulation, avoids carrying and updating the positions of irrelevant

[3]Here, `cl_min/cl_max` is a percentage of in-plane peptides. `cl_min` = 80% $\implies$ 40% cross-linking.

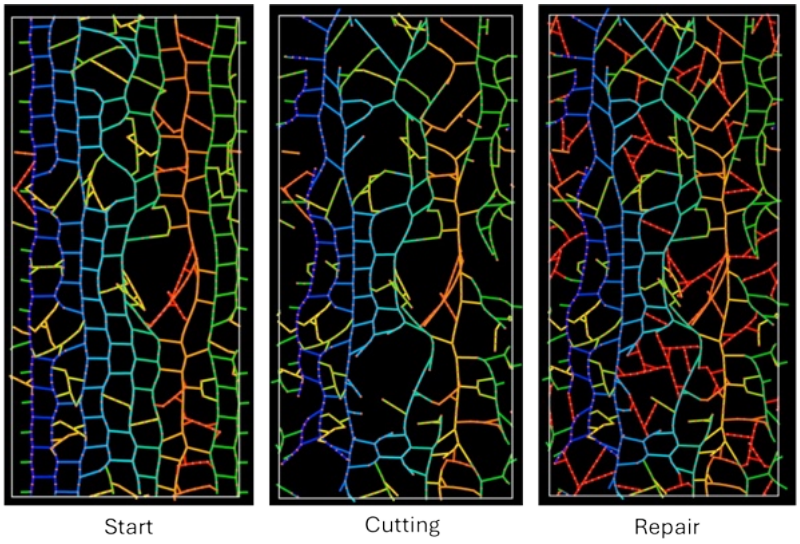

Figure 2.4: (Left to right) Initial system; Random bonds cut and pores form; Pores are filled by the repair mechanism recursively. The newly inserted PG material is coloured in red.

nodes and also mimics the function of breakdown enzymes that are responsible to degrade unsuccessfully inserted or lose strands from the PG layer.

Simulating PG repair

Class A PBPs insert short glycan strands in holes to maintain the structural integrity of the cell wall. When repair is repressed, the cells lyse almost immediately [41], presumably because the large pores allow the inner membrane to bulge through the cell wall, and eventually burst due to the high internal pressure. There must be a certain hole size beyond which the cells lyse, and holes smaller than a few nanometres do not affect the integrity of the cell wall. Thus the PG repair mechanism must have a way to fill holes that are of a certain minimum size.

We implement repair using image analysis techniques to find pores of a certain minimum area in the simulated PG patch, then add an appropriately sized glycan strand along the short-axis of the identified pore, and attach the two ends of a short glycan strand to the appropriate boundary nodes of the pore using peptide bonds. Similar to during insertion, the size of the inserted glycan strands are modulated to minimize the stresses on the boundary of the holes, to reduce artefactual pushing or pulling during repair. (For more details on the algorithm, see section A.2.

Breakdown and repair is illustrated in Figure 2.4).

The simulation

Having implemented each aspect of the PG remodelling system, we simulate the system in the following way. First, an initially disordered system is equilibrated. Then, the pores are repaired, and the lose ends are degraded. With this system,

remodelling events are simulated in a loop as: insertion → repair → random cutting → repair → degrade. After each of these processes, the system is given time to equilibrate. One such loop is called a remodelling event or synthesis cycle. This algorithm is illustrated in detail in the supplementary figure B.1, and snapshots of the simulation are provided at each step in figure B.2.

Chapter 3

Results of the 2DPG model

In this project, we built a computational model of the PG cell wall of rod-shaped gram-negative bacteria, and simulated growth via enzymatic remodelling.

Modelling the three different enzymatic remodelling processes independently afforded us the flexibility to test out many different growth conditions. For example, we were able to toggle the enzymes on and off to mimic drug perturbations, like turning off rod-complex mediated synthesis to mimic A22 treatment (section 3.6), or repair function to mimic cefsulodin perturbations. We were also able to test how our model performs in various conditions such as different pressures, cross-linking degrees and autolytic activity.

3.1 Validating the mechanical properties of the 2DPG patch

A characteristic property of the PG layer is its elasticity, or its Young's Moduli, and it is often used as a key metric to compare models to experimental measurements [15]. Other useful dimensions of comparison between simulations and experimental measurements include the distributions of strand length, bond orientation (i.e. disorder) and pore sizes.

The glycan strand length distributions of the 2DPG model are skewed due to its small size and periodic boundaries. This makes perfect comparison of strand length distributions between this model and experiments difficult. However, using a large system for the simulations, we are able to validate the mechanical properties of the PG layer quite well.

Young's Modulus and the Poisson ratio

In order to validate the elastic properties of the simulated PG patch, we measured its Young's moduli and Poisson ratios in the x and y direction.

The elasticity of a material is a measure of how difficult it is to stretch or compress it along a certain direction. Generally, the elasticity (i.e.Young's modulus) is mea-

sured by exerting a known force along a direction, and measuring the the resulting extension. The inverse of the slope of the force-extension curve gives the Young's modulus for that direction. This is Hooke's law. More generally, Hooke's law relates the stress on a material to its strain. Stress, as described in section 2.1, is the force exerted on the material, per unit perpendicular length over which it is being exerted. Hooke's law when written in terms of stress takes the form:

$$\epsilon_i = E_i \sigma_i \tag{3.1}$$

Where E_i is the Young's modulus or elasticity in along i, ϵ_i is the resulting strain of the system upon a stress of σ_i in the same direction, while all other stresses are 0.

Since the 2DPG system has different stresses and elasticities in the x and y directions due to the anisotropy of the glycan bond orientations, the system we are working with is *orthotropic*. For such a system[1], Hooke's law is generalized as shown:

$$\begin{bmatrix} \epsilon_x \\ \epsilon_y \end{bmatrix} = \begin{bmatrix} \frac{1}{E_x} & -\frac{\nu_{yx}}{E_y} \\ \frac{-\nu_{xy}}{E_x} & \frac{1}{E_y} \end{bmatrix} \begin{bmatrix} \delta\sigma_x \\ \delta\sigma_y \end{bmatrix} \tag{3.2}$$

Where ν_{ij} is the Poisson ratio, which is the negative of the ratio of the strain in the j direction over the strain in the i direction, when stress is applied in the i direction: $\nu_{ij} = -\epsilon_j/\epsilon_i$ [19]. It is important to note the use of differentials here, since the for a system that is already under stress, the Young's Moduli are only defined for local *deviations* in stress.

We start with a perfectly ordered and equilibrated system at pressure P, and then iteratively increase the stress (by changing the set-point described in section 2.2) in the x direction by 0.025% up to a 1% increase while keeping the y stress constant. We then measure the corresponding strains in both the x and y directions. The measured strain in the x direction when plotted against the externally exerted stress gave us the Young's modulus in the x direction (E_x), and when plotted against the measured y strain gave us the Poisson ratio in the same direction (ν_{xy}). This was repeated for the system as the y stress was varied and the x stress was held constant to measure the Young's modulus in the y direction (E_y) and the Poisson ratio ν_{yx}.

This set of simulations gave us the Young's moduli for a given pressure. To see how this changes with pressure, we repeated the above simulations over a series of pressures ranging from 0 to 0.5MPa. The results are shown in Figure 3.1.

When compared against experimental measurements, the perfectly ordered system overestimated the stiffness in both the directions (as seen in Table 3.1). We reasoned that since the real peptidoglycan layer is disordered, increasing the disorder in our system might lead to a closer match. We varied the disorder of the system first by randomly cutting some glycan and peptide bonds, and measured the Young's moduli and Poisson ratios again. Running the simulation multiple times with different initial

[1] ignoring shear forces

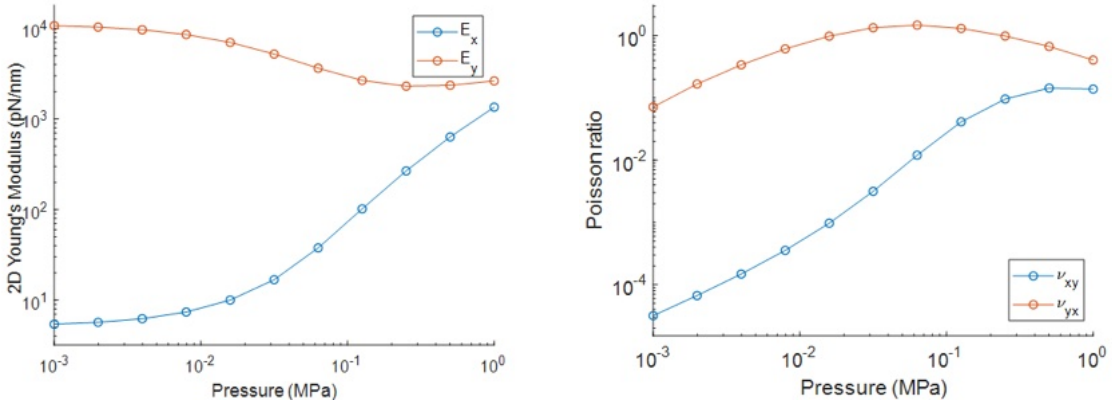

(a) Young's Modulus (b) Poisson ratio

Figure 3.1: Young's Modulus and Poisson ratio calculated in a perfectly ordered system as a function of pressure

cuts, we found that the Young's moduli in the direction of the peptides match closely with experimental values, however the circumferential young's modulus is still larger than expected. It is possible that the infinite glycan strands make E_y much larger than in the real cell. To test this, we used a non-loop insertion simulation[2] to ensure that there were no infinitely long glycans looping around the patch. Indeed, upon measuring the Young's moduli for such a system, we saw a much better match of the stiffness along the glycan strands (E_y) between our simulations and literature.

The results of these simulations are tabulated in Table 3.1, for pressure = 0.1MPa. To compare with experimental data and other models, we assumed the thickness of the PG layer to be 3nm, which is within the reported range of the thickness of the peptidoglycan sacculus [45] [15] [9]. Values in the literature when measured in MPa, were converted to the units of pN/nm used in this study by multiplying the literature values by PG thickness.

Pore-size distribution

Using AFM, Turner et al. [36] imaged the PG cell wall in *E.coli*, and were able to extract a lot of detail about the structure of the cell wall, such as the bond orientations and pore-sizes, which is another good metric of comparison for models in the literature [15].

In order to avoid edge effects and have a good representation of the steady-state of the 2DPG system, we took a 256 subunits long simulation, and ran it for multiple insertion events. At steady state, the network was extracted, and is shown in Figure 3.2. The pores are calculated using the same methods used in section A.2. Because we find pores in the 2DPG patch only based on the positions of the nodes (rather than the bonds), any gaps with a pore diameter less than the typical length of a bond (3-4nm) is ignored from the analysis.

[2] A simulation where all the infinitely long glycan strands are randomly cut at one location before insertion

Model	E_y (pN/nm)	E_x (pN/nm)	ν_{yx}	ν_{xy}
AFM [45]	105-180	45-90	0.48	0.16
AFM [9]	87-207	45-93	0	0
GU-inf [15]	637	34.8	0.30	0.018
GU-non-inf [15]	187	18	0.363	0.062
2DPG (perfectly ordered)	2669	101	1.31	0.04
2DPG (disordered)	1347	**110**	0.15	0.07
2DPG (non-inf simulation)	**151**	5.1	-1.65	0.10

Table 3.1: Comparison of Young's moduli (YM) and Poisson ratios from literature measured at around 0.1MPa, to our measurements. We convert the Young's moduli reported in MPa into pN/nm by dividing the YM in MPa by the thickness of the pg layer (3nm). AFM: experimental measurements from Atomic-Force-Microscopy; GU-inf: Model by Gumbart et al. with infinitely long periodic glycan strands; GU-non-inf: Model by Gumbart et al. without any infinitely long glycan strands. Bold numbers show values from our simulations that match with experimental measurements.

We see that in steady state, the general distributions of pore sizes in the 2DPF model (Figure 3.2B) look comparable to experimental pore-size distributions in from the literature [36](Figure 3.2).

Taken with the comparison of Young's Moduli, these results show that the 2DPG model's mechanical properties match experimental values, and hence afford us some confidence that the 2DPG approximates the real cell wall to a good degree. It is also a testament that the empirically determined parameters have been chosen well, such that the system now resembles a real cell wall.

3.2 A mechanism for persistent width reduction

Furchtgott et al. had proposed in 2011 that pre-stretching the glycan strand by approximately 10% before inserting it into the PG network [12] can result in a conserved width, while pre-stretching it more can cause width to reduce. However from back-of-the-envelope calculations of the forces required to stretch a glycan strand by that much, it is hard to enzymatically justify such strong stretching energies within the cell: For a stiff glycan bond with stiffness constant of $\approx$ 5000 pN/nm [26], pre-stretching the bond by 10% of its relaxed length would require 500pN of force. While molecular motors can exert forces in the order of 10s of pN [11], they are not enough to cause the stretching required to achieve the desired insertional pre-stretching. Furthermore, no such motors are known in the periplasm, nor is ATP available as an energy source. It is possible that there are some other conformational-change or Brownian-ratchet based mechanisms that the cells use to pre-stretch glycan strands during insertion, here we propose a mechanism for width reduction without stretching glycan bonds during insertion.

Following the make-before-break strategy of glycan insertion (section 2.2), where

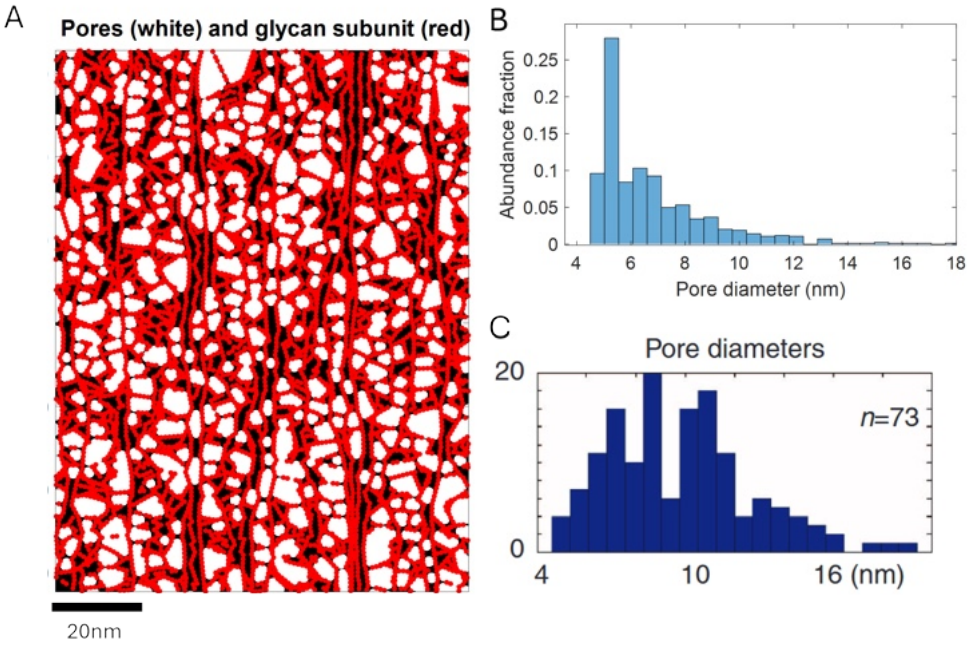

Figure 3.2: Pore-size distribution in the steady state of a 256 subunit long system. A: Pores (white) and the glycan subunits distribution (red) after about 17 insertion rounds. B: The histogram of pore sizes, with a filter at 4nm. C: Experimental pore diameters from [36].

new peptide cross-links on the glycan strand are made before any other bonds are cut, we propose that sparse cross-links and coordinated synthesis and cutting can lead to a steady width reduction while maintaining length elongation. When the newly inserted glycan bond zig-zags due to the tension on the peptide cross-links along the x axis, it constrict in the y direction and expands the x axis. This alone might cause the width of the entire system to reduce by a small amount, but it will not lead to a consistent width reduction. To achieve a continued width decrease over many insertions in our simulations, we propose that if the kinking of newly inserted glycan strands eventually constricts the width more than the length of a single glycan subunit, the next inserted glycan strands will have one less subunit. Being smaller in length, this strand would carry most of the stress in the y direction and and constrain the width. This cycle can then repeat where the new glycans kink and further reduce the width.

To test whether the glycan strand kinking upon underlying bonds being cut is enough to reduce the width of the system, we separated the insertion of the strand from the cutting of the bonds underneath it.

As expected, we saw that when the underlying glycan and peptide bonds are cut, the stress is transferred onto the new strand, which bends and causes the width to reduce significantly Figure 3.3. Unexpectedly, we see that just insertion also has a substantial effect in reducing width, which means that just cross-linking alone is causing enough kinking for the width to reduce. This implies that the search-radius of the rod-complex while looking for available peptide stems is large enough

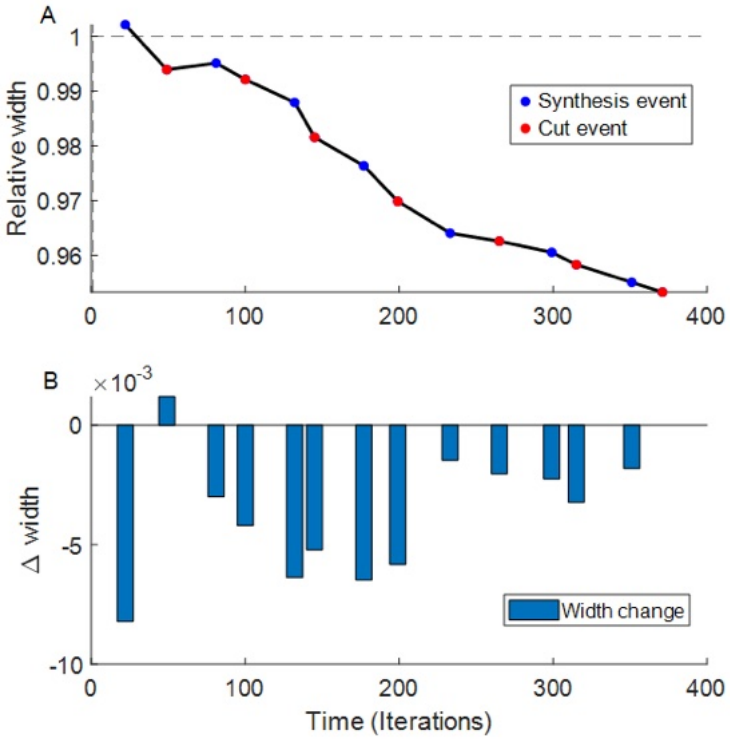

Figure 3.3: Both, the cross-linking of newly inserted glycans and the cutting of underlying bonds cause width reduction. (Top) Relative width of the simulated patch against the number of insertion events (remodelling events) shows a consistent width drop caused by both just insertion and just cutting. (Bottom) Bar-plots of width reductions caused by each insertion and subsequent cutting shows that both insertion and cutting lead to comparable width reductions.

to reduce width. This effect can be tuned by changing the search radius in the rod-complex within a certain range. Search radii that are too large, lead to strands 'reaching over' adjacent strands to cross-link to glycans further away. This pulls the system in length, and ends up inhibiting cell elongation. On the other extreme, a search radius smaller than half the typical distance between adjacent glycan strands can lead to the newly inserted strand only cross-linking on one side.

Over many insertions that simulate a cycle of insertion, repair and degrade, we see a strikingly consistent width reduction, supporting our hypothesis of newly inserted glycan strands driving width reduction via the zig-zagging mechanism (Figure 3.4).

In a real cell however, the long glycan strands are not infinite loops, and so the floppy peptides at the ends of the strands may stretch easily and constrict the glycan strand without having as much of an effect in constricting the width of the cell. For sustained width reduction in this case, the kinking would need to compensate for the peptide stretching at the ends. Naturally, the effect the the peptides at the ends have on the glycan constriction reduces as the length of the glycan increases. So, we would expect that for a large enough system, the glycan strands would be long

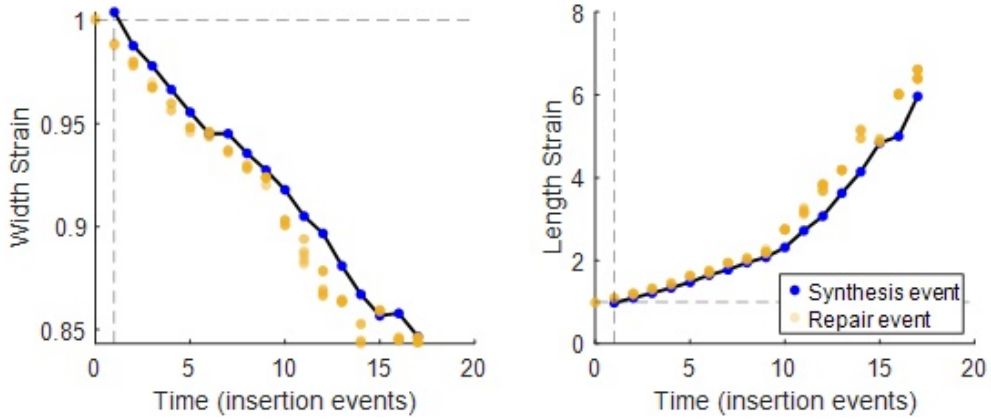

Figure 3.4: Width reduces consistently over many insertions. Figure shows relative width (left) and length(right) normalised to the initially equilibrated system and plotted against the number of insertion events (remodelling cycles). Over multiple cycles, the width reduces at approximately 5% every doubling.

enough such that even though they have relatively floppy ends, the constriction due to kinking more than compensates, and the width would still reduce.

We tested this hypothesis out by only inserting non-looping glycan strands in a large[3] system. This was done by randomly cutting one glycan bond in the newly inserted glycan loops the moment it is inserted. As expected, for a large enough system size, the widths continue to reduce robustly (Figure 3.5).

Upon comparison with experimental values, the rates appear very similar. Hyper-osmtic ramp experiments have shown that cell widths change plastically, and when looked at as a function of length, the ratio of changed width to change length, the strain ratio, gives us an idea about how quickly the widths are changing. For hyper-osmotic ramps, the strain ratios were consistently 0.02 [27]. Even in nutrient shift experiments as well as our own experiments described in section 4.1, we see a consistent shift width change a rate of 5% per length doubling. The simulations match this rate quite robustly, also showing an approximately 5% change in width per doubling. However as we will see in the next chapter, this rate is determined by various parameters.

3.3 Exploring the parameter space

Experimentally determined parameter values are very important for the 2DPG model to be able to mimic the real world as well as possible. Over the last few decades, the understanding of the PG material has improved considerably [7][43][15], where researchers have been able to determine characteristic mechanical properties of the PG layer quite well. Turner et al. used AFM to determine the pore-size distribution, orientation, disorder and the distribution of length of glycan strands across the cell, while other studies such as Deng et al. [9] and Shin et al. [31] have

[3] 256 subunit long

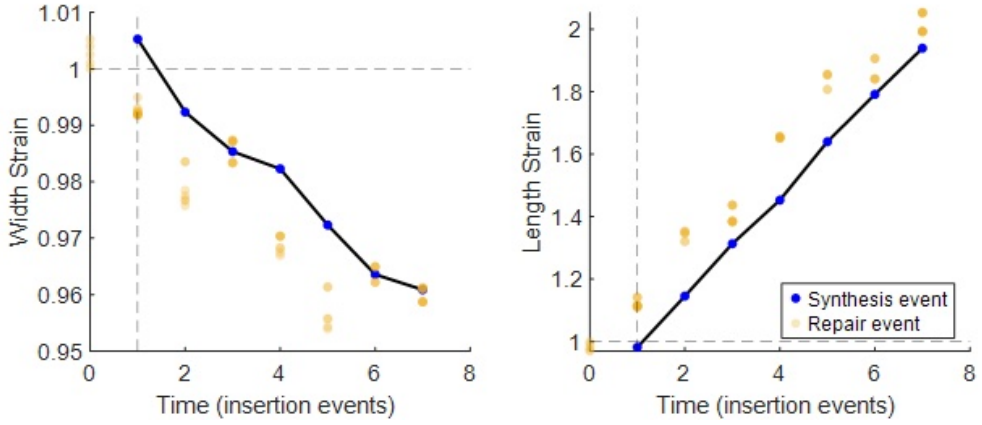

Figure 3.5: Large patch sizes with 256 nodes along the y axis show consistent width decrease with non-looping long glycan strands. Non-looping glycan strands means that while the system is still under periodic boundary conditions, the long glycan strands do not loop around the whole patch. There is at least one break along the long glycan strands in the initial system, and also during insertion. This mimics a real PG layer better than the ones with the infinite glycan loops.

experimentally measured the elastic properties of bacterial cells. In a preceding section (section 3.1), we showed that using these physical parameters, the mechanical properties of the 2DPG model agrees quite well with experimental data, giving us some confidence that our simulations approximate the PG cell wall well.

However, parameters like the autolytic cutting rates or the degree of cross-linking have not been experimentally measured, and can only be empirically guessed. Unlike the physical properties of the PG layer, these remodelling parameters, including the turgor pressure, may have regulatory mechanisms constantly controlling them based on the cell's environment and growth conditions. For example, *S. Typhimurium* growing inside other eukaryotic cells has a reduction in overall degree of cross-linking [13] and *E.coli* cells show sudden changes of turgor pressure upon nutrient shifts despite a constant medium osmolarity. [27]. Even for parameters that can be measured like osmotic pressure, what is really measured is the relative pressure difference in the cell because measuring absolute pressure in the cells is not yet feasible. Additionally, variability due to the cell themselves regulating pressures leads to very broad ranges of turgor pressure estimates, ranging over an order of magnitude from 0.03MPa to 0.3MPa [9].

Thus, we do not know exactly what values to set such parameters at, nor do we really understand how cell widths depend on each of these parameters. In order to gain some insight into the effect of the degree of cross-linking, internal pressure, and peptide and glycan cutting rates independently on the widths and lengths of the cell, we systematically varied these parameters in our simulations. In these cases, it is more instructive to see how the width changes as a function of length, since the ratio of the width and lengths strains is a real measurable quantity, while the insertion events are a feature of this model and is difficult to assign a discrete measurable event to.

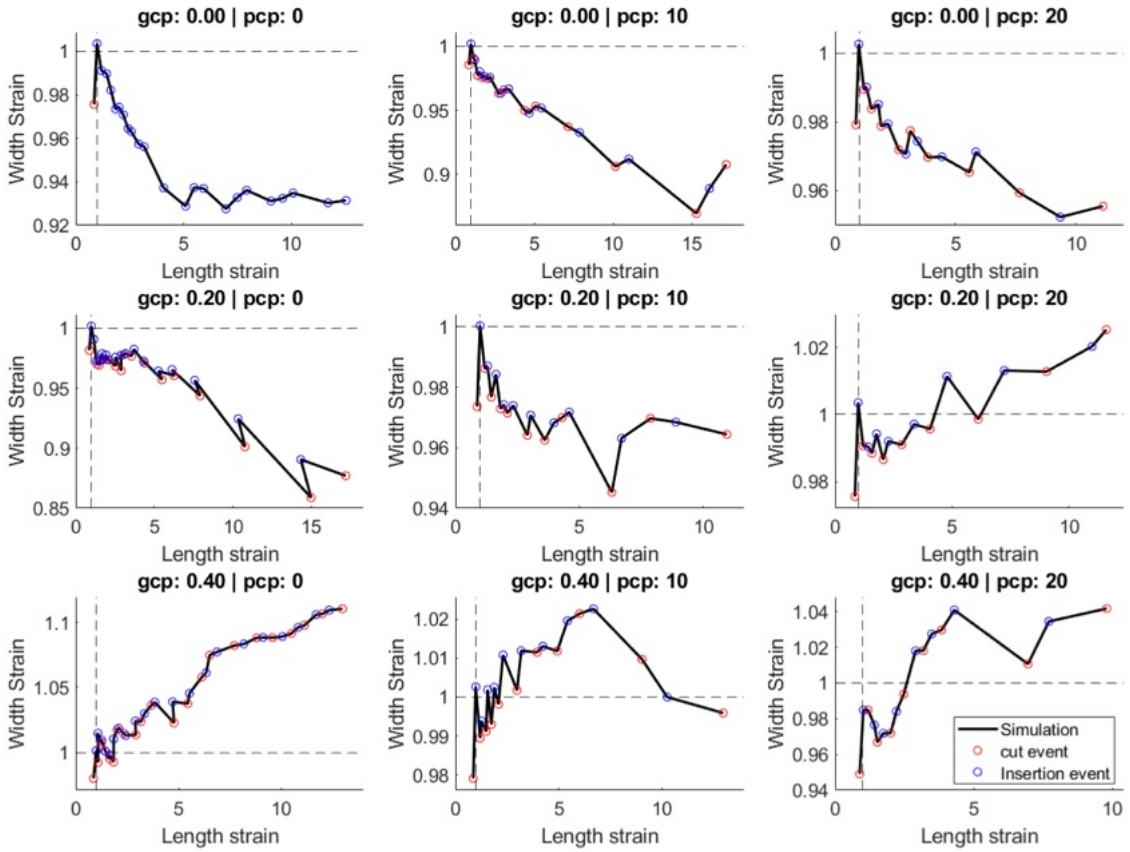

Figure 3.6: Simulation run at 0.03 MPa with a range of cutting frequencies. Glycan cutting rates are varied from 0% to 0.4% (top to bottom), and peptide cutting rates are varied from 0% to 20% (left to right).

Cutting rates and their effect on the number of long glycan strands

Cutting glycan strands causes width to increase dramatically. Exploring different peptide and glycan cutting rates for a system in Figure 3.6, we see that for low peptide cutting, as the glycan cutting percentage (gcp) increases, so does the width. However, things get a lot more stochastic when both glycan and peptide cuts are made. A clear trend for the peptide cutting percentage (pcp) is not immediately apparent, but a lose trend of width increase from the top left to the bottom right of Figure 3.6 implies that broadly, cutting increases width.

We had expected that higher pcp would lead to a faster length increase. This is not obvious from Figure 3.6. However, when the lengths are plotted against the number of insertion event completed, we see a very clear trend. Three simulation trials are overlayed in the supplementary Figure B.5 to show that higher pcp leads to a faster length increase of the system. This implies, as expected, that it is majorly the role of the peptides to hold the system together in the lateral direction.

The infinitely long glycan strands constrict the width of the cell in our simulations. So in order to understand how quickly we lose the infinite glycan strands on randomly

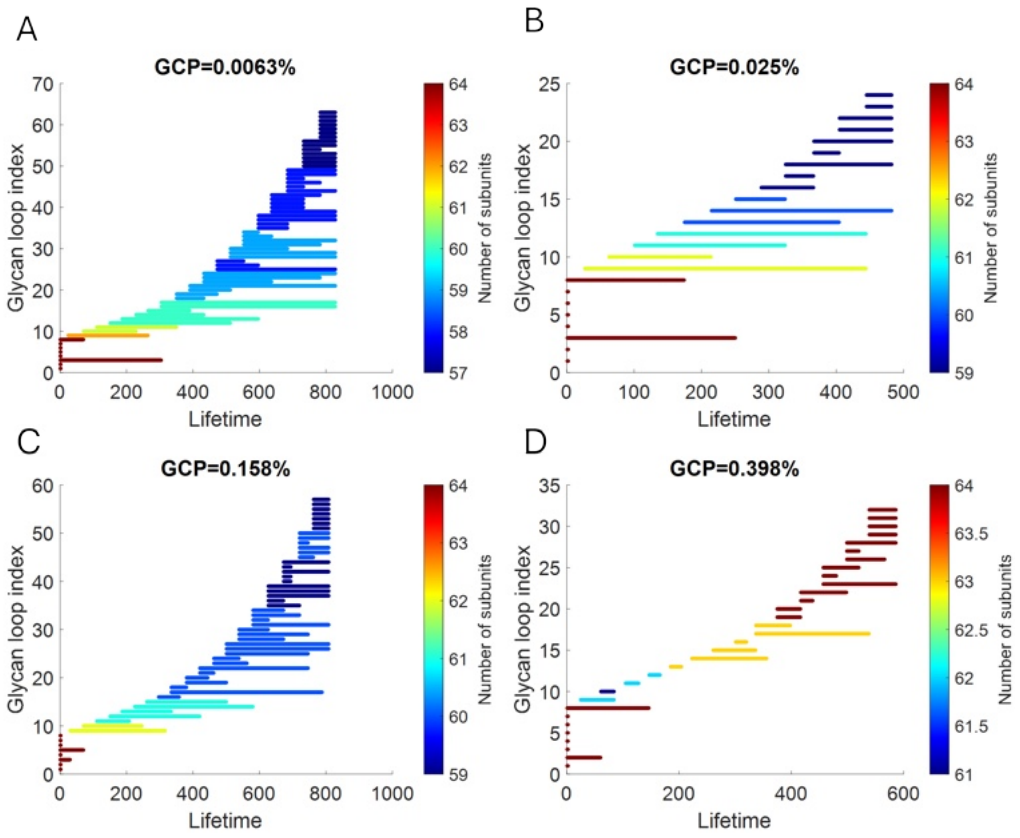

Figure 3.7: Glycan lifetimes as a function of glycan cutting rates. Each line here represents the lifetime of a long glycan loop. The colorbars represent the number of nodes in the loop (or its contour length).

cutting a given percentage of glycan bonds, we plotted the lifetimes of the glycan loops as a function of time in Figure 3.7. Here, a line begins at the insertion of an infinitely lone glycan strand, and terminates when the strand get cut. We see here, that beyond 0.25% cutting, glycans seem to be cut the very soon after their insertion. This is why, for simulations where the gcp is more than 0.2%, the widths are able to grow quite quickly. In this figure, the colour of the line indicates the number of subunits in that glycan strand. When we see the colour of the newer glycan strands becoming blue from red, this implies that the width of the system is decreasing. Similarly, when the colours go from red to blue, the widths are increasing.

From this, we proposed that perhaps the density of glycan strands also can determine whether the widths increase or decrease. While these results are still preliminary, in Figure B.3 we see that for high glycan cutting, the glycan densities are also lower. Empirically, I notice that when the glycan density is above 0.1 strand per nanometre, widths decrease, and vice versa. If this is a real result or a coincidence is not clear yet, and more work is required to have this kind of a concrete threshold, if any exists.

The effect of cross-linking and pressure

We also systematically varied pressure and cross-linking amount across simulations, as shown in Figure 3.8. Here, we increased the cross-linking by changing the `cl_max` and `cl_min` of the system (see section A.2. As pressures increased from 0.01MPa to 0.1MPa (top to bottom in Figure 3.8), we saw that the strain ratio reduced, meaning that the amount of width reduction per length increase become smaller, and then for a pressure of 0.1MPa, width actually began increasing with length. While this behaviour might seem intuitive at first, it is not immediately obvious why the 'zig-zag' mechanism does not work at higher pressures. We try to understand this phenomenon using a simplified theoretical model of the glycan strand along with some more experiments in the next few sections (section 3.5).

Unexpectedly, we did not see a clear monotonous pattern in the amount of width constriction as the amount of cross-linking was increased. Logically, we expected that as the cross-linking increased, the amount of kinking would not be very substantial, and this would cause the width reduction to slow. To have an intuition about this, consider a taught vertical thread, which is being pulled perpendicularly to the right from a point along its length. As you can imagine, the thread would kink from the point of pulling by a certain extent. Now, say you pull the thread from another point towards the left. As you increase the points along its length where you're pulling left and right, the amount of kinking will reduce, because the perpendicular forces will begin cancelling each other out as they get denser. For infinite such points, the thread should remain perfectly straight.

From our simulations, instead of this effect, it looks like the width reduction is strongest for an intermediate cross-linking amount, compared to the low and high. As in the case of pressure dependence, we used a theoretical model to better understand how the amount of cross-linking affects the zig-zagging behaviour, and why this un-intuitive dependence on cross-linking arises in our simulations.

3.4 Simplified model of a glycan strand

To have a sustainable width decrease, the system needs to constrict in the y direction enough to be able to fit fewer glycan subunits in a loop, in the next few iterations. It follows that for a sustainable width decrease, the kinking mechanism needs to be able to theoretically cause a width reduction of more than 100/`nrow`%, where `nrow` is the number of un-stretched glycan nodes that can fit into the system. This number is higher in a real system where the glycan strands are not 'infinite' loops, and the edge effect of the stretchy peptides makes it harder for the kinking to constrain the width of the system (see section 3.2).

Even in the ideal case while dealing with infinite glycan strands, it can be instructive to understand how much a glycan strand needs to bend or kink to be able to sufficiently reduce the width, and is this theoretically possible, given that the y stress is 2 times the x stress. In order to explore this, we develop a simplified model of a perfectly ordered glycan strand that is cross-linked by peptide bonds.

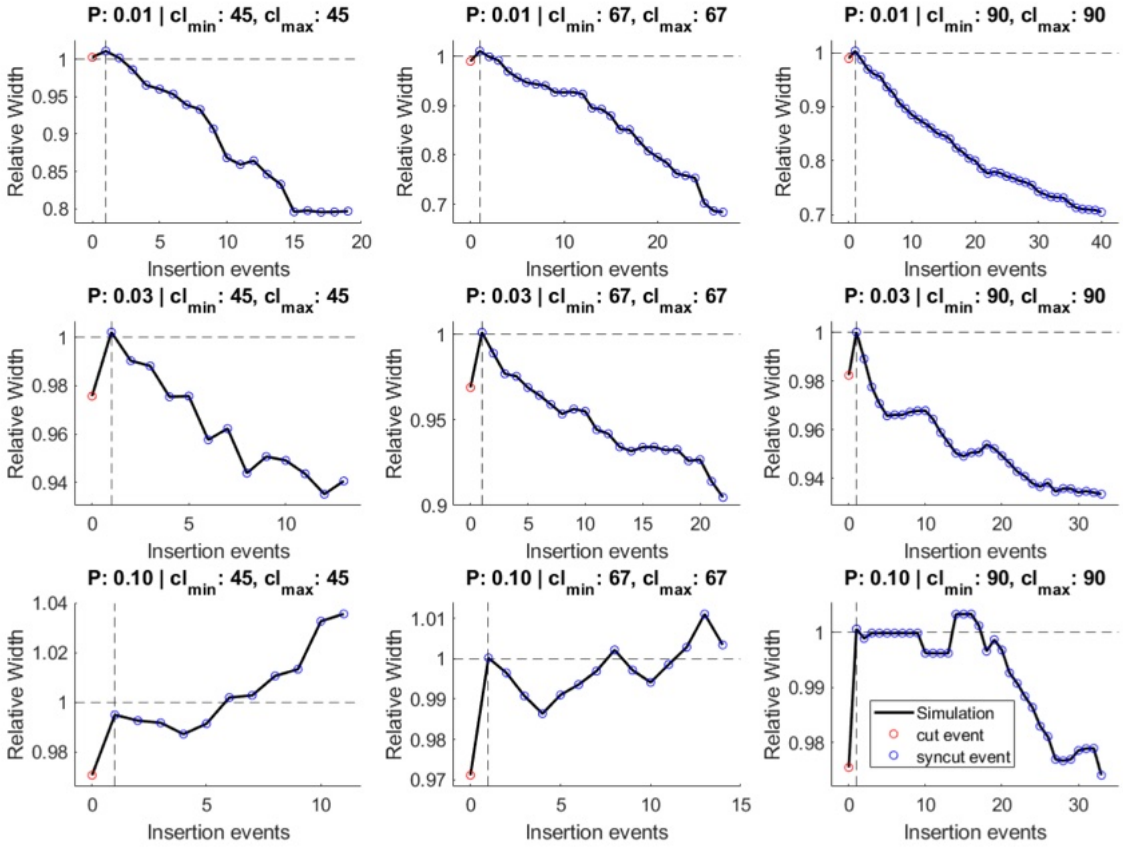

Figure 3.8: Simulation of many insertions as pressure is increased from 0.01MPa to 0.1MPa (top to bottom), and peptide cross-linking is increased from 45% to 90% of the theoretically expected peptide cross-links (left to right).

For our general system size of 64 subunits in width, the amount of width reduction required is at least 1.5%, and as the width reduces, this percentage keeps rising. The following toy model helps us with guidelines towards two questions:

1. Does the number of cross-links on the new strand matter?
2. Does the lateral density of glycan strands matter?

Does the number of cross-links matter?

Let N be the number of cross-links on each side of the strand, as shown by the blue dashed lines in Figure 3.9C. Additionally we define α as the angle between each glycan bond and the vertical axis, l as the contour length of each glycan strand, x as the end-to-end distance in the x-axis of the strand (including the l_p nm long peptide stems i.e. half a peptide bond being used to cross-link the strands), and y as the end-to-end length of the strand along the y-axis.

For simplicity, we assume that neither the glycan bonds nor the peptide cross-links are stretchable, and that the system is periodic in the y axis. $l_g = l/2N$, where l_g is the effective bond length of a glycan bond. From some basic trigonometrics, we

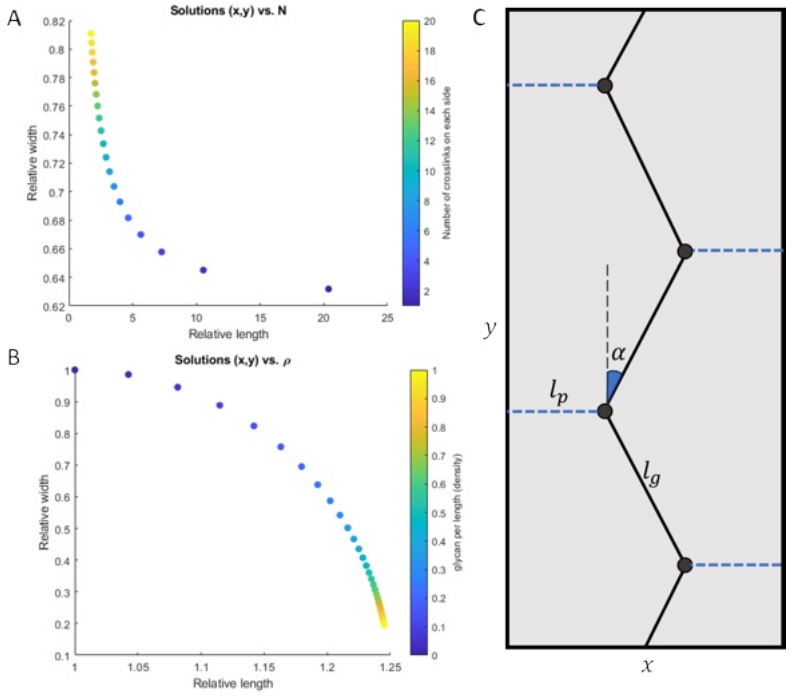

Figure 3.9: The theoretical toy model for a glycan strand. (C) shows a schematic of a typical periodic glycan strand in a perfectly ordered network. The number of peptide cross-links (blue dashed lines) on each side is given by N, and the rest of the properties such as system size in x, y and angles are as labelled. (A) shows how the system dimensions change at equilibrium conditions as a function of cross-linking number, and (B) shows the same as a function of glycan density.

can also write x and y in terms of system parameters as:

$$x = l_g \sin(\alpha) + 2l_p \tag{3.3}$$

$$y = 2Nl_g \cos(\alpha) \tag{3.4}$$

As we change N, we are effectively changing l_g. Assuming that the contour length or the number of glycan subunits in the strand remains fixed, reducing N means reducing the number of kinks along the strand, and thus increasing the size of the glycan between the cross-links, which is nothing but l_g.[4]

Since the strand is a small part of a cylindrical cell, the stress in the x and y directions are given by equation (2.6). The stress in the y direction is twice the stress in the x direction. Converting the stress to forces on the strand using $F = \sigma l$, where $l = x$ or y, and dividing it equally by the number of cross-links or supports, we get

$$F_x = \frac{\sigma_x y}{N} \tag{3.5}$$

$$F_y = \sigma_y x \tag{3.6}$$

We also have the relation between the angle α and the forces as $\tan(\alpha) = F_x/F_y$. Plugging in equation (2.6), we get:

$$\tan(\alpha) = \frac{\sigma_x y}{N\sigma_y x} = \frac{Pry}{2NPrx} = \frac{y}{2Nx} \tag{3.7}$$

Thus, we get a simple toy model that relates the angle that the glycan strand makes to the number of cross-links. The higher the angle, the more the strands are kinked, and thus lower the width (y).

From the simulations, we estimate the the average α is in the order of 10°. We can thus approximate the model using the small angle approximations. After some algebra, we get:

$$x = l_g\left(\frac{y}{2Nx}\right) + 2l_p \tag{3.8}$$

$$y = 2Nl_g\sqrt{1 - \left(\frac{y}{2Nx}\right)^2} \tag{3.9}$$

The square-root term is then expanded using the Taylor series, and the higher order terms are dropped:

$$x = l_g\left(\frac{y}{2Nx}\right) + 2l_p \tag{3.10}$$

$$y = 2Nl_g\left(1 - \left(\frac{y^2}{8N^2x^2}\right)\right) \tag{3.11}$$

[4]Care needs to be taken here to not confuse l_g with the length of an un-stretched glycan subunit.

This shows us that as we increase N, initially the width drops quickly, and eventually reaches an asymptote.

This is also what we see in the finger-trapping simulations (Figure 3.11), where alternate peptide cuts show more of the constricting effect because alternate peptide cuts effectively leads to a lower N. The behaviour in the simulations are more complex because this model assumes that the bonds don't stretch, and as a result, this model is independent of the pressure. However in the real system the pressure increases the glycan stretching, and that can lead to width increasing too. In fact, the finger-trapping effect seen as pressure is increased in section 3.5 explores exactly this effect.

Does the glycan density matter?

We can model glycan density by distributing the stress in the y direction over more or fewer glycan strands. This means that for a given stress, if there are more glycan strands per unit lenght in x, each of the glycan strands will be under a smaller force; carrying a smaller fraction of the stress.

Let ρ_g be the number of glycan strands per unit length in the x direction. Thus, the force on each glycan strand in the y direction F_y becomes

$$F_y = \frac{\sigma_y}{\rho_g} = Pr/\rho_g \tag{3.12}$$

From the earlier equations, we then get $\tan(\alpha) = \rho_g y/2N$, resulting in a model in terms of both glycan density and crosslink amount:

$$x = l_g\left(\frac{y\rho_g}{2N}\right) + 2l_p \tag{3.13}$$

$$y = 2Nl_g\sqrt{1 - \left(\frac{y\rho_g}{2N}\right)^2} \tag{3.14}$$

As can be seen in Figure 3.9B, as we increase the glycan density, the relative width is further reduced. This can be interpreted as glycan strands that are close together work together to reduce the width - with more glycan strands (per unit length), it gets easier to reduce the width.

3.5 Understanding width dynamics using a toy model

Finger trapping behaviour

At lower pressures, the width of the system decreases plastically, but at higher pressures, it increases (Figure 3.8). Initially, we had expected that as pressure increased, the stress on the glycan strand cross-links would lead to more kinking, causing the width to reduce. However, here opposite effect was observed, suggesting that increased pressure does not necessarily increase glycan zig-zagging.

Since it was unexpected, we wanted to understand the mechanics of the 2DPG network in a little more detail. We examined its equilibrium configuration of the 2DPG network with varying degrees of disorder as a function of increasing pressure. Focusing on a static network[5] at different pressures, we measured its steady-state widths and lengths relative to those at zero pressure (Figure 3.10).

Based on the results shown in Figure 3.8, and the previous discussion, we now anticipated a monotonic increase in both length and width with increasing pressure.

As expected, the system's length increased monotonically with pressure, since higher pressures push the system outward. However, the width exhibited the behaviour we had initially guessed: at first, as pressure increased, the equilibrium width of the cell (L_y) constricted. Only after reaching a certain pressure did the width start to increase (Figure 3.10). This unexpected behaviour is reminiscent of the Chinese finger-trap toy and has been observed in bacterial cells before [4].

We hypothesize that this initial constriction is due to the glycan kinking mechanism (section 3.2). At higher pressures, the the glycan strands stretch considerably, and this results in a length increase that overpowers the kinking effect, causing the width to begin increasing.

This provides some justification as to why we see width reduction only at some pressures even in a full PG simulation. When a new glycan strand is inserted and cross-linked, it behaves essentially like a glycan strand in Figure 3.11. Depending on the stresses on the x and y axes, this glycan strand stretches and kinks, and this results in a net constriction in the y axis for lower pressures, but a net expansion at higher pressures.

A toy model for stretching and bending helped us understand this behaviour and the dependence of other parameters like the disorder amount or cross-linking along a glycan strand (as described in section 3.4). The model shows that reducing the cross-linking should make the effect of constriction more pronounced. This was already seen in Figure 3.10, because the higher disordered patches mimic lower cross-linking. We noticed that typically, as the disorder increased, the finger-trapping effect increased with it. However, since the system size is small, the stochasticity brought from cuts being in different places is what makes this plot so noisy at higher disorders.

As an additional test, we also were curious about how the stiffness of the glycan strands affected this effect. Across the board, stiffer glycans showed a more pronounced effect, as well as shifting the minima of the finger-trap towards higher pressures.

To test the effect of cross-linking more explicitly and without the stochasticity of randomly disordered systems, we cut every alternate peptide cross-link, and re-ran the simulations over a range of pressures (Figure 3.11). Indeed, we saw a much more dramatic reduction in width when the cross-link amount was reduced in a perfectly ordered network.

[5] A network without any enzymatic remodelling

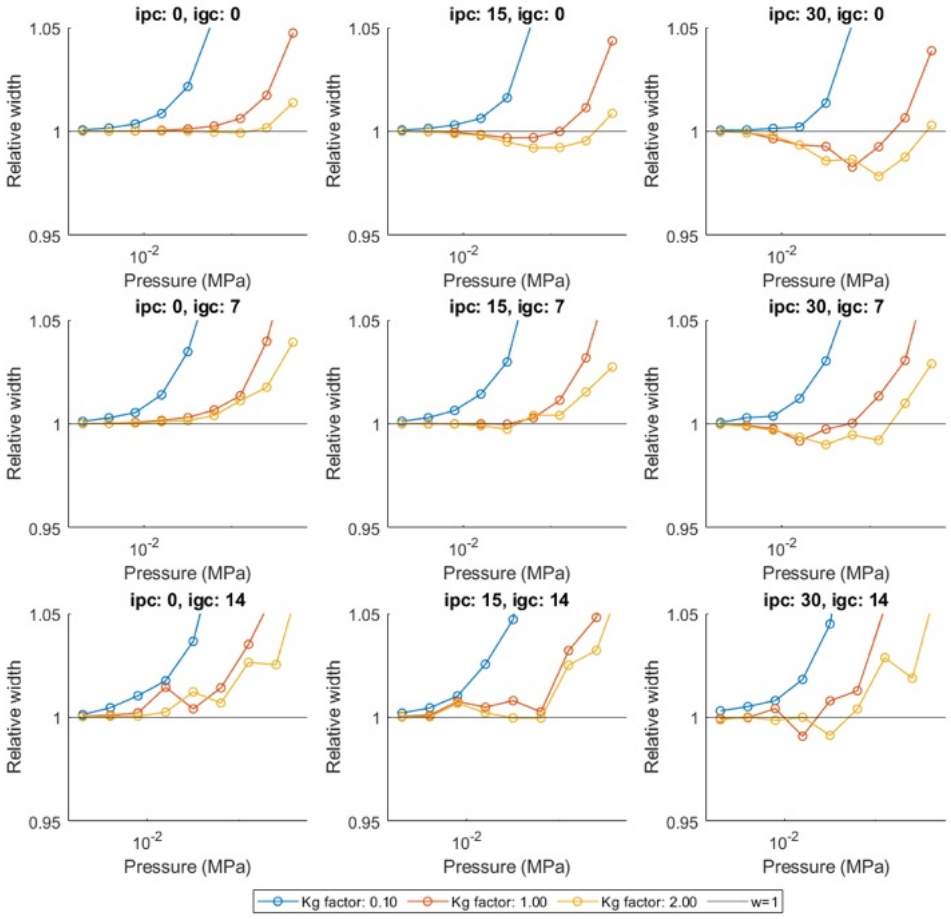

Figure 3.10: Finger-trapping effect with increasing pressure: Static simulations (without enzymatic remodelling) of PG networks with various levels of initial disorder and glycan stiffness. Here, ipc stands for 'initial peptide cuts' and igc stands for 'initial glycan cuts' corresponding to how many bonds were cut at the start of the simulation, Kg factor is the factor that is multiplied to the glycan stiffness to alter its stiffness, For each initial starting condition, the final equilibrium dimensions are measured at varying pressures.

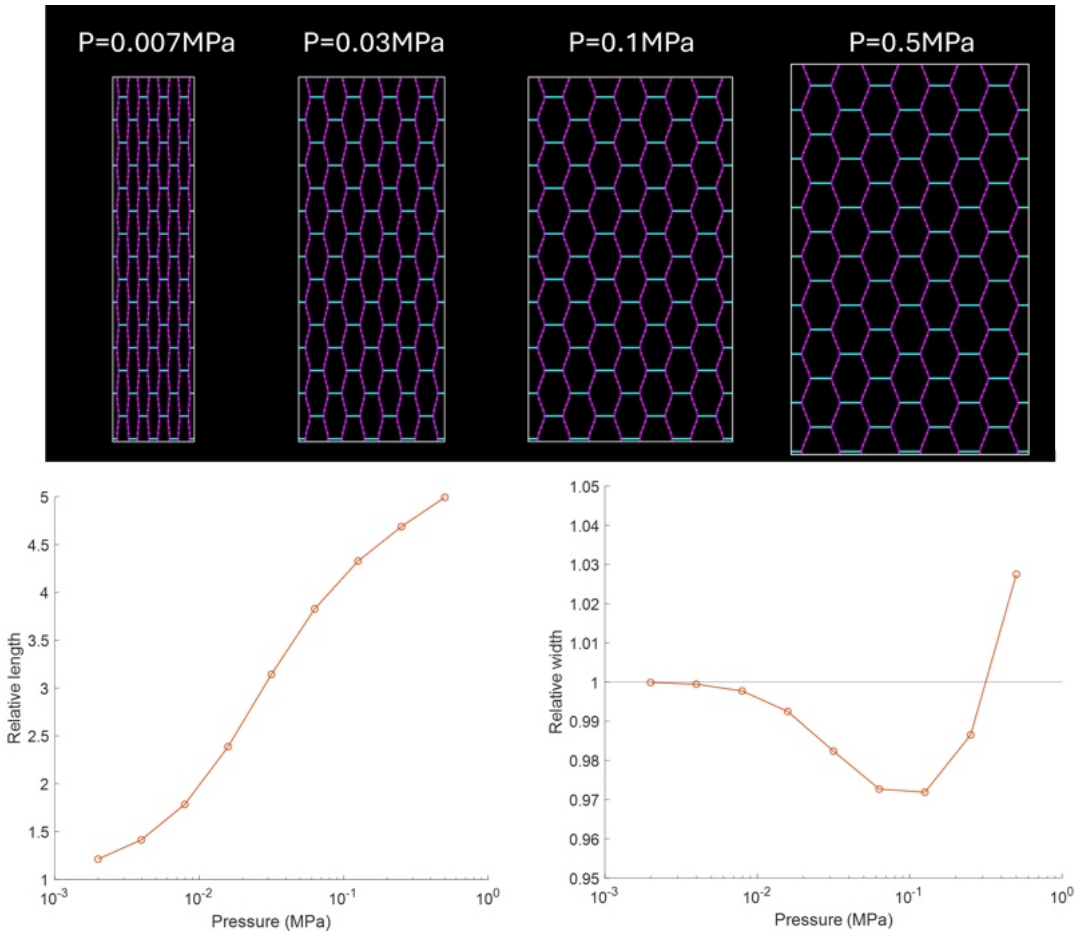

Figure 3.11: A sparse PG network in which every alternate peptide bond is cut exhibits a much stronger finger-trapping effect as pressure increases. (Top) Screenshots of the system's final configuration at different pressures show that the width (y-axis) initially decreases and then increases. (Bottom) Plots showing how the length and width vary with pressure.

Toy model and the Pressure-Crosslinking matrix

From the toy model in Section 3.4 and our results in Figure 3.11, we expected that increasing cross-linking in newly inserted glycan loops would lead to a decrease in width reduction per insertion. Specifically, we anticipated that width would decrease rapidly at low cross-linking but more slowly at high cross-linking, because increased cross-linking (N) leads to a much larger finger-trapping effect Figure 3.9. However, Figure 3.8 does not show this trend.

This lack of effect becomes clearer when considering the relationship between cross-linking and length growth. Higher cross-linking reduces the kinking of newly inserted glycans, slowing down length increase. Since length growth is proportional to the x-component of the glycan contour, the contribution of each glycan strand, given by Equation (3.8) and Figure 3.9A, decreases as cross-linking increases. As a result, higher cross-linking leads to a higher glycan density in the x direction.

From Equation (3.14) and Figure 3.9B, we see that increasing glycan density leads to greater width reduction. Therefore, the expected trend does not appear in the simulations because the higher glycan density counteracts the effect of increased cross-linking, resulting in nearly constant width reduction rates. In other words, two opposing effects almost seem to cancel each other out: Increased kinking and width reduction due to lower cross-linking, and decreased width reduction due to a lower lateral density of long glycan strands.

3.6 Inhibition of Rod-complex activity

A22 is an antibiotic that inhibits the polymerization of MreB, which is required for rod-complex mediated glycan insertions. A22 treatment does not cause cell lysis, but it results in the cells losing their rod shape, and become spherical. Time-lapses of *E.coli* cells with A22 treatment show that the width is seen to increase quickly; 50% increase in width, within one doubling time [27].

From systematic variation of gcp similar to the work described in section 3.3 but not shown here, we found that for our system of 64 subunits in width, and Pressure of 0.03MPa, the widths remain conserved (neither increase not decrease) at a gcp of $\approx 0.25\%$.

We simulated A22 treatment in the 2DPG model by letting the system grow normally for a few insertions at a gcp such that the width remain conserved (gcp=0.25%), and then turning rod-synthesis off and simulating for a few more insertions. We repeated this for a range of peptide cutting frequencies to see the effect of peptide cutting on system dimensions (Figure 3.12.

As expected, width increased. For larger peptide cutting percentages (pcp), the length strains were larger, while for 0 pcp, the length of the system did not grow.

Some estimates of our system with 8 initial glycan strands show that when pcp is 0, the peptides that are cut due to the rod complex insertion (syncut) function initially are at around 5-7%, but within 5 insertions, make about 1-3% of the peptide bonds

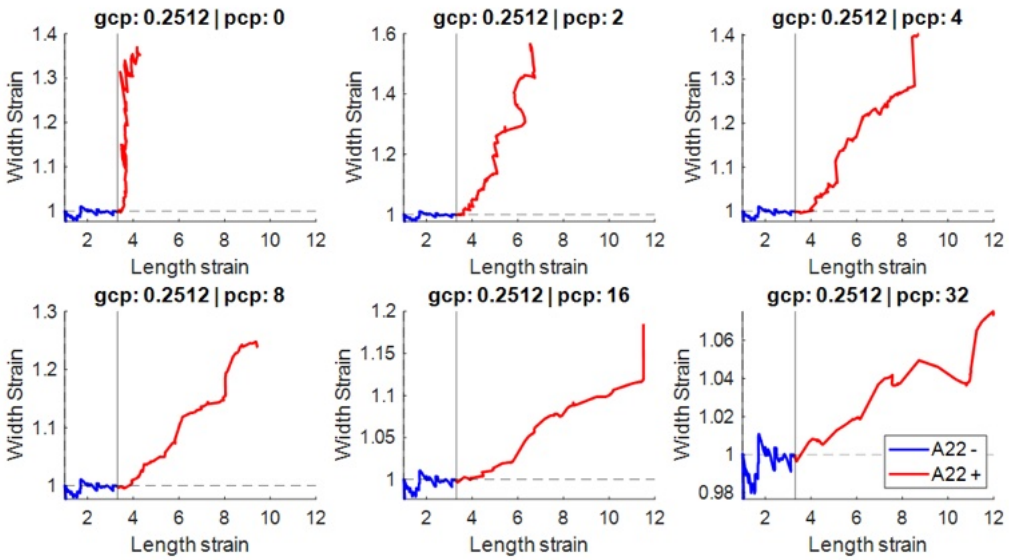

Figure 3.12: Simulated A22 treatment: Let system grow normally (blue) and then stop rod-complex activity (red) for a range of peptide cutting frequencies. All the blue lines are from the same simulation; i.e. they are identical.

in the system. In other words, even with 0 random cutting, at steady state, the pcp is effectively 1-3%. Remarkably, looking at the pcp=2% plot in Figure 3.12 on the top centre, we see a width increase of 50% in about one doubling time, fitting very well with experimental data.

While it is still early to tell, this might imply that the baseline cutting rate by the hydrolases is somewhere around 1-3% of all available peptide bonds, which is a very reasonable number, and also comparable to our estimates of the baseline glycan cutting rate, which we estimate to be around 0.2%, at which width is seen to be pretty well-maintained.

Chapter 4

Experiments

Over the course of the project I set up some preliminary experiments. However, due to time constraints and focusing more on developing the 2DPG model, I present only a subset of these experiments here.

As mentioned earlier, A22 is an antibiotic that inhibits rod-complex activity, causing cells to lose their rod shape and increase in width by over 50% in less than one doubling time. To understand how environmental factors influence width regulation, we investigated the effect of pressure changes on the rate of width increase after A22 treatment in filamentous *E.coli* cells. We started the experiment but were only able to complete two control conditions: one without any pressure change and another with a 700 mOsm hyperosmotic ramp, which led to a 5% width decrease in one doubling time. This experiment is briefly described in section A.5 in the appendix.

In another experiment, I try to recreate a result from Bardetti et al. [4], where they show finger-trapping like non-linear behaviour in *B.subtilis*, similar to what we see in Figure 3.11. This experiment is also briefly outlined in the appendix in section A.4.

4.1 Defect chasing

Cells can plastically change their widths within a generation timescale. It is also known that long filamentous cells maintain a consistent width along their length. However, the physical scales over which width regulation operates are not well understood. For example, does the entire cell width change uniformly along its length, or do localized bulges and constrictions form? What are the characteristic spatial scales of bacterial width regulation?

We hypothesized that if a characteristic scale exists, small width deformations along the cell length should be corrected within a generation timescale, and also appear somewhat regularly along the cell-length.

Using phase contrast microscopy, we measured the widths of SulA induced *E.coli*

cells for up to two hours, and then used Morphometrics to segment the cells, extracting width data for each cell along its length. Making kymographs to visualise the width heterogeneity along the cell length, we see that width defects (slight bulges or constrictions) have a lifetime, and aren't immediately corrected. The defect corrections even within a cell is of the order of a doubling time, and remarkably, cells that appear to constrict in one part can simultaneously increase in width in another part.

Method

E.coli MG1655 cells with pDB192 plasmid with SulA inducible by IPTG are grown at 30°C in Lysogeny Broth (LB) overnight. The overnight culture (OC) is then diluted to an optical density at 600nm (OD) of approximately 10^{-4}, and allowed to grow until exponential phase is reached will be called the Diluted Culture (DL). The culture is diluted occasionally to make sure that the OD does not exceed 0.3. LB-Agar pads are prepared in parallel by mixing 10mg Ultrapure Agarose into 1ml of LB, and poured into 1mm thick moulds, and allowed to cool for 30 minutes.

1μl of the DL at OD 0.1 is pipetted on an ibidi glass slide, and a 1cmx1cm square section of the 1mm thick agar pad is placed carefully on the cells, avoiding bubbles. Finally, the cells are imaged under a phase contrast microscope for 2 hours. Images are analysed using Morphometrics [31], an open source software for cell segmentation.

Results and discussion

Figure 4.1 shows the variation of width along a cell as a kymograph. Here, the width at each point on the centre-line of the cell is depicted as a function of time. As can be seen, small defects appear in the cell width; bulges or constrictions, which are of the order of 1 μm in size. These defects are seen to reduce with time, and also spread out over the length of the cell, in the timescale of one generation. For example, in Figure 4.2A, a bulge appears at t=3min at which point the width at that location is 1.20 μm. In approximately 30 minutes, the width rises to 1.2μm (a 2% increase in width in a little less than one doubling time). Within another doubling time, it spreads out over the length of the cell, and also reduces in magnitude to the width returning to 1.2 μm.

We also see in cells that within the same cell, there can be parts of the cell where the width is constricting while others where the width is increasing as seen in Figure 4.2B. in 25 minutes, the width went up from 1.183 µm to 1.22 µm. This was a 2% weight increase in less than one doubling time. At the same time in another part of the cell we saw the weight decrease from 1.15 µm to 1.082 µm, which is about a 5% drop.

In both the cases, we see a similar physical scale of approximately 1 μm, and a temporal scale of 25 minutes; approximately one doubling time.

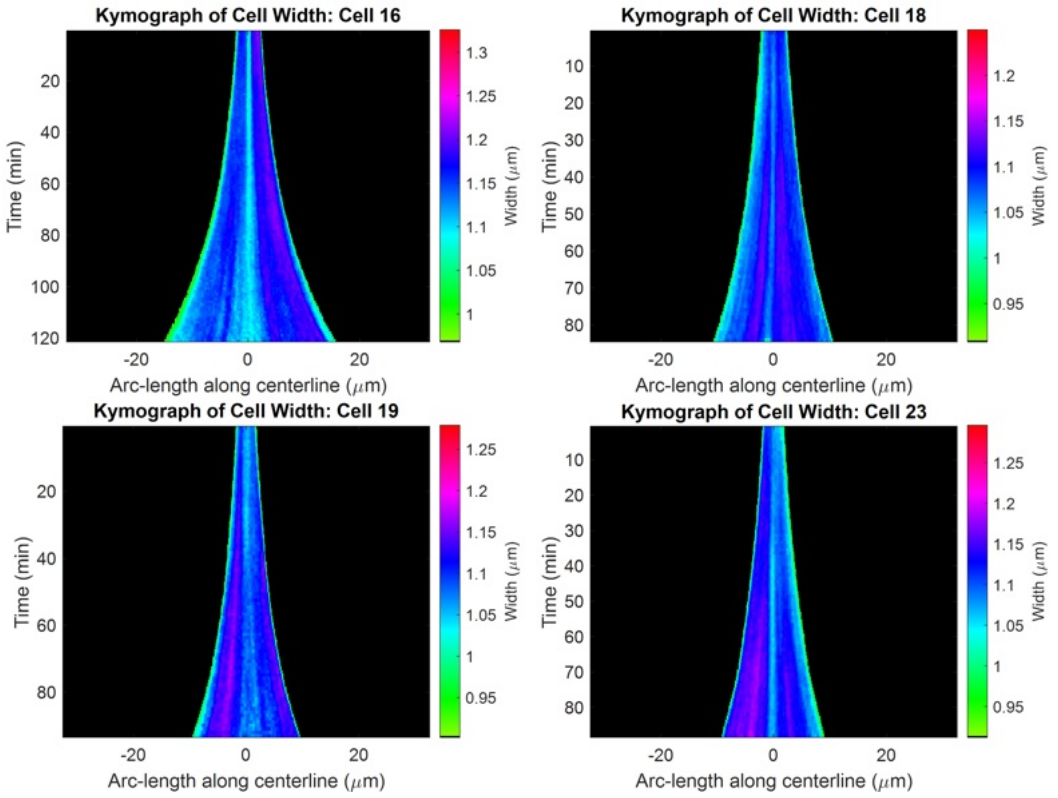

Figure 4.1: Kymograph plots of width along the cell's centerline (cell length) for SulA induced MG1655 *E.coli* cells. Magenta streaks correspond to width bulges that form and disappear in the timescales of 40 minutes, and light-blue streaks show constrictions. The central light blue streaks show the incomplete division septum. All images are analysed from phase contrast microscopy.

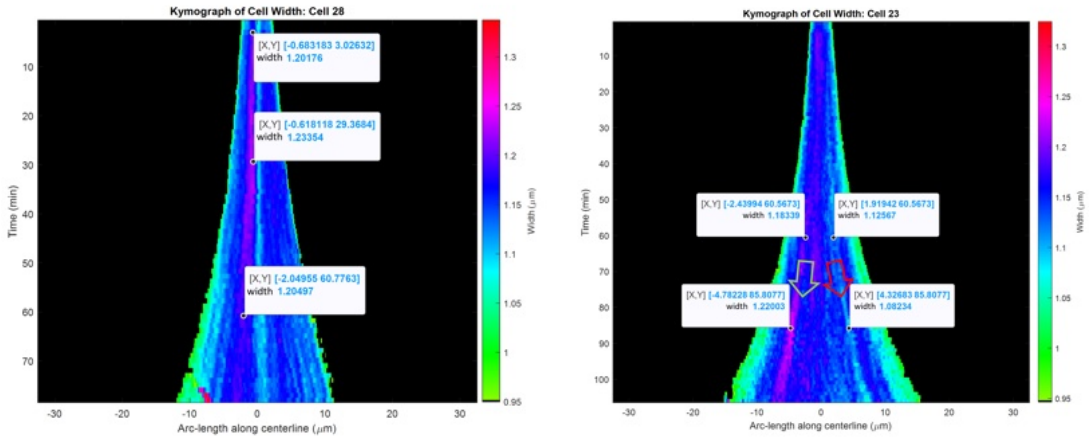

(a) (b)

Figure 4.2: Width kymograph similar to 4.1. (a): The emergence and dissipation of a local bulge in cell width between t=3 min and t=60 min. (b): Two regions in the same cell, one where cell width is increasing showing a magenta streak, and the other where cell width is constricting, showing a cyan streak. The green arrow corresponds to the direction of increasing width, and the red arrow to decreasing width. Data points are highlighted to be able to read the width off easily.

4.2 Hydrolase activity without MreB

Recent experiments in the lab showed that the overexpression of endopeptidases causes width reduction by more than 5% followed by lysis. This was repeated by overexpressing in *E.coli* a hyperactive mutant of ShyA (endopeptidase native to *Vibrio cholerae* [31]), MepS, and a hyperactive mutant of MepM (both of which are native endopeptidases in *E.coli* [13]).

It is not intuitive why the cutting of random peptide bonds in the peptidoglycan layer can lead to a systematic reduction in cell width by such an amount over the length of the cell, especially since in our simulations the cutting of random peptide bonds did not seem to have much effect in reducing the cell width. Since many of the peptide bonds in the cell are not connected to long circumferentially oriented glycan bonds, it is hard to imagine how randomly cutting them can cause these bonds to kink and width to reduce enough, while also avoiding the formation of large pores due to "irrelevant" peptide bonds being cut.

While it is possible that class penicillin binding proteins (aPBPs) find the pores extremely fast and repair them before the cell actually lysis in the early stages of the endopeptidase over-induction, I think it is unlikely that that is the mechanism here.

In the simulations, we had to cut the peptide bonds that are directly above the newly formed glycan strands, to transfer the stress on the cell wall onto the new strands and drive width reduction. We hypothesized that perhaps it is the function of these endopeptidases to only cut those peptides that are directly under the newly

inserted strands. As such, I reasoned that the endopeptidases could be co-localised spatially or functionally with MreB or the Rod complex, such that only the relevant peptide bonds are cleaved, and this cleavage can drive width reduction.

To test whether peptides are only cut where there are new glycan strands, we thought to stop the addition of new glycan strands using A22, which de-polymerises MreB. This would cause there to be very few or a decreasing number of available "newly inserted" glycan strands. Then if the endopeptidase is overexpressed, it would not have a lot of sites where it can cleave the peptidoglycan layer, and thus we would see a reduction in the lysis rates.

Method

To test this, we set a growth curve experiment where we used MG1655 strains with plasmids containing the MepM mutant, ShyA mutant and wild-type cells, and looked at the growth rates upon induction of the endopeptidase using 1% arabinose and 10μg/ml A22. For controls, we had only A22, only induction, and none. If the hypothesis is correct, we would expect the A22 + arabinose treatment to show reduced lysis as compared to just arabinose treated cells.

Results and discussion

Opposite to what we had expected, the cells with A22 treatment as well as arabinose showed an increased rate of lysis as compared to just arabinose. Only A22 treatment showed no lysis at all (Figure 4.3).

Looking at the MepM treatments (Figure 4.3 column 1, row 2), we see that only MepM over-iduction reduces the OD a little, and the A22 makes the effect much stronger. Meanwhile, in the case of ShyA over-induction (Figure 4.3 column 1, row 3), the addition of A22 does not change the growth rates by much, presumably because the ShyA overinduction already reduced the ODs to almost 0.

This is easily seen in the second column of the figure, where we can see that the action of ShyA is stronger than MepM in row 2. However, ShyA+A22 and MepM+A22 both behave identically, despite the differences in the action of the hydrolases alone. This is a puzzling result.

One interpretation of this data could be that endopeptidase activity is more fatal when the rod-complex is inactive or when MreB is de-polymerised. But it could also imply that the activity is more pronounced when MreB is not there. Concretely, it could be that endopeptidase makes the same number of cuts on the cell wall in both cases, and with A22 the cuts lead to faster lysis. Or, that without MreB, there are more cuts made on the cell wall.

One hypothesis I have is that A22 treatment causes the PG layer to become more disordered, which results in the stresses being more equally distribution among the bonds. Most probably, this happens by reducing the stress on the long glycan bonds, and increasing the stress on peptide bonds. If endopeptidases work in a stress-dependent way where they cut only those peptides that are stressed, the A22

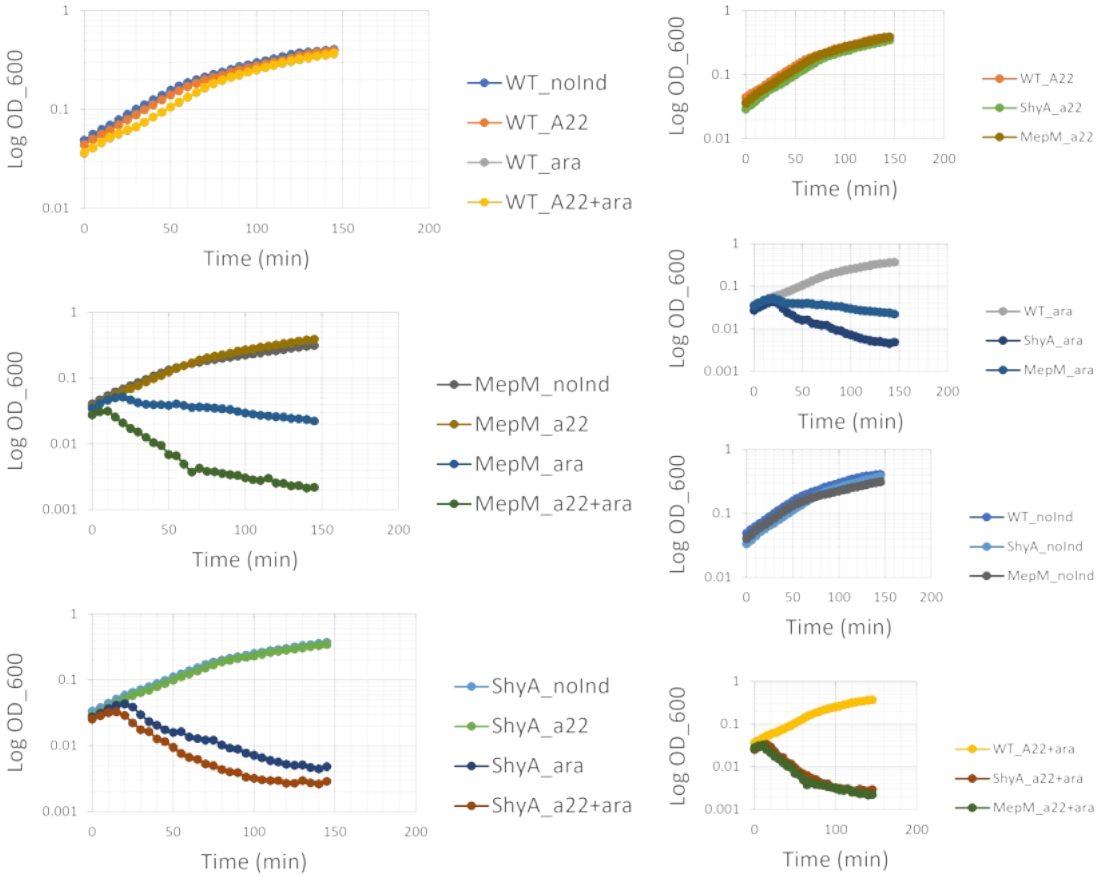

Figure 4.3: Hydrolase and A22 co-treatment. overactive mutants of ShyA and MepM are induced in MG1655 cells in the presence and absence of 10μg/ml A22. As control, cells without any induction or treatment, and cells with only A22 treatment are also compared. To measure the lysis rates, OD_{600} is measured every 5 minutes. (column 1) The data grouped according to Hydrolase. (column 2) The data is grouped according to treatment type.

treatment would indeed result in a higher fraction of 'stressed' peptide bonds, which might show the kind of result we are seeing. This hypothesis is supported by other fragmented bits of information, such as how we see an increase in width growth rate at higher pressures, possible because there is an increased rate of cutting, and the fact that I think it is unlikely the cells actually randomly cut bonds, as this might lead to the cleavage of really important bonds and eventual lysis. The fact the we don't routinely see spontaneous lysis of growing cells implies that which bonds are cut are probably regulated somehow.

Chapter 5

Discussion and future directions

Discussion

Cell widths are remarkably conserved, and for a given species and growth medium, the variation in cell widths in a population is only about 5%. At the same time, the widths appear flexible when the cells are subjected environmental perturbations by changing their cell widths into a new steady state in the timescales of less than one doubling. Despite decades of research on cell shape, how cells display such precise width control while also showing pliancy upon environmental perturbations remains unknown.

Cell shape is determined by the peptidoglycan cell wall. It forms a rigid scaffold around the cytoplasm, enabling the cells to withstand high intracellular turgor pressures and protect the cell from environmental threats. The cell wall, made up of glycan polymers cross-linked to each other by peptide cross-links, makes a covalently linked net-like structure around the cell, and can only grow or change its shape via the effect of enzymatic remodelling.

PG remodelling enzymes can cut older material, and insert new PG material. However, how cells use cutting and insertion of PG to control cell width is still an open question. Specifically, how nanoscopic enzymes are able to coordinate to accurately control a macroscopic property like cell shape and width has been debated for a few decades.

Seminal work by Nguyen et al. in 2015 showed how a templated insertion of glycan strands by an enzyme complex can lead to maintained cell widths for many cell doublings [26]. However, the templated nature of insertion along with the existence of only one enzyme complex that did everything did not allow for cell width control wherein the widths could increase or decrease based on environmental cues. Following recent discoveries that show that the cutting enzymes (autolysins), Rod-complex and the cell-wall repair enzymes (aPBPS) work semi-autonomously [8], this work employs computational methods to model the PG layer and the independent enzymatic processes, to propose a mechanism that the remodelling enzymes might use to be able to increase, maintain or reduce their widths.

A small section of the cylindrical part of a rod-shaped bacterium was simulated as a perfectly flat, periodic network of glycan strands cross-linked by peptide bonds. Both the glycans and peptides were approximated by springs following the work by [26]. Long glycan strands were simulated as infinitely long glycan strands, which looped around the width of the patch (y axis) and connected back to itself. The formulation of the model is explained in detail in Chapter 2.

Having verified that the simulated cell wall patch shows mechanical properties similar to real cell walls, as seen from atomic scale models and experiments (Table 3.1 and 3.2)[1], we moved on to simulate enzymatic remodelling: Autolysis, Repair and Rod-complex mediated insertion independently.

We hypothesized that when long, circumferentially oriented glycan strands are inserted in an unstretched state and cross-linked laterally, they bend under the tension from peptide cross-links. This bending causes the strand to adopt a zig-zag shape, effectively shortening its projected width-wise length (along the y-axis). As more such bent strands accumulate, they collectively generate a passive constrictive force on the cell wall. Once enough of these strands are present, the continued insertion and cross-linking of straight, unstretched strands could lock in the reduced width. These newer, unbent glycans would resist any expansion, as stretching them would require overcoming the stiffness of their bonds.

The hypothesis was tested following Figure B.1, where the dimensions along the y and x axis of the patch correspond to the width and length of a rod-shaped cell respectively. Simulations of PG showed a persistent reduction in width for many length doublings at a remarkably constant rate of 5% per doubling (Figure 3.4), corroborating the plausibility of our proposed mechanism of width reduction. Through this work, it is demonstrated for the first time that the width of a cell can be constricted without the need for additional enzymes exerting constrictive forces (as was proposed earlier [12]). Additionally, the work presents a spatial (but not necessarily temporal) coordination between autolytic activity and the rod-complex, which can be tested experimentally using single-particle microscopy of tagged MreB and known autolytic enzymes in live cells. The rate of width reduction matches measurements from environmental perturbations and osmotic shock experiments [27].

Cells growing in different mediums and upon different environmental and drug perturbations have different intracellular pressures [21]. Upon simulating the system at different pressures, we saw widths decreasing for lower pressures, but increasing for pressures of more than 0.1MPa 3.8. Further investigation on the nature of the PG material showed an interesting non-linear effect of pressure to the degree of kinking in the glycan strands. When the enzymatic remodelling was turned off (Figure 3.10), the inert patches of PG showed a 'finger-trapping' like effect, where increasing the pressure caused a reduction in the equilibrium width, and then increasing

[1]The circumferential Young's modulus is overestimated in our models probably because of the effect of infinitely long glycan strands that make the system very stiff in the Y direction. When measured with a system with no glycan loops, we found that Young's moduli match closely with experimental results.

again.

We propose that this finger-trapping behaviour of the PG layer determines at which pressures insertion of long glycan strands can reduce cell width. When a long glycan strand is inserted into the PG layer, it is initially not under any tension. However, when the underlying bonds are cut and the glycan strand is incorporated into the cell wall, it suddenly experiences stresses in both x and y directions. This system behaves like an inert PG layer as modelled in Fig. 3.10. Depending on the pressure in the system, whether these stresses will cause the strand to kink and reduce its length in the y direction, or stretch and increase it, can be essentially predicted from the figure based on whether the relative width is lesser or greater than its value at zero pressure.

The use of looping glycan strands traversing the width of the simulated patch constrains the width increase a lot more than they would in a real cell. In our simulations, the width cannot increase against the stiffness of the glycan strands unless glycan strands are cut. Meanwhile, in a real cell, the glycan strands do not form hoops around the circumference, and so they have some leeway to slide past one another and allow for more flexibility in width.

While the difference in flexibilities may not be large between the simulation and the real cell (section 3.1), it affects the amount of kinking that is required for the consistent width reduction mechanism. As described in section 3.2, the width reduction due to kinking needs to be at least as much as the peptide stretching. For example, if we consider non-infinite glycan strands, the edges of the glycan strand would be held in place by the peptide bonds, which are much more flexible than the glycan strands. Thus, upon kinking, while the glycan strand itself might considerably reduce in width, it might not pull the rest of the patch with it, since the peptides would just stretch instead. For a persistent width decrease then, the constriction in the glycan length would have to be enough to cause make up for the stretching of the peptides.

Both the previous concerns are addressed by large system size simulations, where the inserted glycan strands are long, but not looping. We tested the effect of non-looping glycan strands by randomly cutting one glycan bond in all the infinite loops in a simulation and then inserting non-looping glycan strands. While we saw consistent and appreciable width decrease for a 64 subunit long patch in the case of infinite glycans, we required a system size of 256 glycan subunits in the y direction to see persistent width reduction 3.5. This fits remarkably well with the persistence length of MreB filaments reported in [40] and also the length of the long glycan strands as measured by [35], demonstrating the need for the insertion of *long* glycan strands for width maintenance. This further corroborates the importance of the Rod-complex in maintaining rod shape, since only the rod-complex mediated insertions are capable of such long glycan strand insertions.

In real cells, autolysins cut bonds in the PG layer, while aPBPs and the rod complex insert material. As expected, cutting and insertion were shown to have opposite effects on the cell width, where cutting lead to an increase in width, while rod-complex mediated insertion lead to a decrease in width (Figure 3.6 and Figure 3.12).

Thus, it is conceivable that the way cells 'regulate' their widths are by essentially regulating their autolytic activity. For the cells to grow wider, they can upregulate hydrolysis, and for the cells to grow thinner, the cells can downregulate autolysis and let the effect of the rod-based insertion take over in constricting the cell.

As it stands, we cut all bonds that cross the newly inserted glycan strand. However, if only a subset of these are cut, there may be an opportunity to slowly build a multi-layered PG cell wall, mimicking gram-positive bacteria. Hence, this model can allow us to probe questions about how gram-positive bacteria might change their enzymatic mechanisms to be able to regulate their widths too. Moreover, instead of cutting random bonds, bonds can be cleaved based on their age (for example not cleaving the newly inserted glycan strands which can be identified by the presence of penta-peptide stems; untouched by carboxypeptidases), or based on the mechanical stresses they carry. This might give us some flexibility in trying to understand the different roles of the many autolysins available to cells, and also why they become redundant despite subtle differences.

We were able to use the theoretical toy model of the glycan strand (section 3.4) to then understand why and how cutting caused the finger-trapping to increase its effect in Fig. 3.11 and in 3.10 as we increase the initial disorder. We were also able to establish the role of glycan density, and how glycan density and cross-linking amount affect each other negatively, and effectively are able to cancel each other's effect out (Figure 3.8). It is worth noting that the 2DPG simulations are stochastic (Figure B.4), and many simulations need to be repeated multiple times to get average data.

The 2DPG model successfully simulated A22 treatment (Figure 3.12), which matched experimental data remarkably well. From setting the glycan cutting frequency such that the widths don't change much, we estimated that the baseline cutting frequency of glycan bonds might be in the vicinity of 0.2% of all glycan bonds. From estimating the number of de-facto peptide bonds being cut during the rod-mediated insertion, we estimated that the baseline peptide cutting frequency must be at least around 1%. Comparing then, the rate of width increase in the simulated A22 data to actual width increase from experiments, we were able to suggest a baseline peptide cutting frequency of about 2% of all peptide bonds.

We estimated that the enzymatic remodelling is able to reduce width at a rate of about 5% in one generation from our model, and also from the rates of width change from perturbation experiments [27]. This was then confirmed at a sub-cellular scale, where we saw width control at similar rates along the cell length within the same cell 4.1. We also saw width defects of the order of 1-2 microns in these filamentation experiments, implying that the spatial scale of width control is of the order of one micron. These undulations happen almost independently across the length of the cell, meaning that the cell widths are probably not affected globally at the same time, but local changes in width eventually accumulate to have global effects.

Our simulation assumes that the rod complex is uniformly distributed. However, these micron-scale undulations in width point towards there being regions of differential rod-complex activity. Since such regions are still much larger than our simulated

system size, we remain confident that within such a region, the remodelling enzymes can be treated as 'well mixed', and our predictions hold.

Limitations and future directions

While there are only a few empirically determined free parameters in the model, some sensitive parameters like the search radius of the peptide cross-linking or the minimum and maximum number of cross-links per strand are hard to test experimentally, and for now can only be estimated indirectly.

Cells must have a feedback loop to control the set-point for their width. However, in our simulations, the widths either keep reducing, or keep growing. We suspect that the cells might be regulating the glycan strand density in some way to control its width, and are currently working on some theories about how the cell might be doing so, including stress-dependent bond cutting, age-dependent bond cutting, and also transcriptional/translational regulation. Having understood how the cell might change its width, a well developed mechanism of width homeostasis would be very useful in understanding when the cells decide to change their steady state width, and based on what environmental cues.

While the periodic boundary conditions are useful in approximating the behaviour of the long glycan strands in the peptidoglycan layer, they fail to capture the variation in widths along the cell length. Thus, it is not clear from these simulations alone whether the width along the length of the cell would remain conserved for a substantial time. To be able to better test the kinking mechanism of width constriction in more realistic cells, a 3D model of the cell sacculus would be much more ideal, although computationally very expensive. Modelling the insertions as we have in this work on a system similar to the ones developed by Nguyen et al. [26] or Furchtgott et al. [12], it would be clear of the width control can be uniform along the cell.

Another limiting factor of our model is that the pressure range within which the width decrease is seen is in the lower end the reported turgor pressures [9]. It is possible that some of the other physical parameters like the stretching or bending rigidity lead to a bias for lower pressure. It would be good to explore the effect of parameters such as bending and stretching rigidities of the glycans to understand how these affect the system, and if they influence this bias for low pressure.

The model in its current state is flat and small, and thus lacks the ability to comment about larger scale defects along the cell wall. It could be very interesting to expand this model into a full-sacculus model in 3D, where it would then be possible to probe many new properties of the cell, such as bending upon external stresses [1], or even comment on local perturbations in width as in section 4.1. A 3D model would also expand the scope of the model to understand the PG remodelling mechanisms in gram positive bacteria, which have much thicker PG layers.

References

[1] Ariel Amir, Farinaz Babaeipour, Dustin B. McIntosh, David R. Nelson, and Suckjoon Jun. Bending forces plastically deform growing bacterial cell walls. *Proceedings of the National Academy of Sciences*, 111(16):5778–5783, April 2014. Publisher: Proceedings of the National Academy of Sciences.

[2] Shiladitya Banerjee, Norbert F. Scherer, and Aaron R. Dinner. Shape dynamics of growing cell walls. *Soft Matter*, 12(14):3442–3450, 2016. Publisher: Royal Society of Chemistry.

[3] Manuel Banzhaf, Hamish CL Yau, Jolanda Verheul, Adam Lodge, George Kritikos, André Mateus, Baptiste Cordier, Ann Kristin Hov, Frank Stein, Morgane Wartel, Manuel Pazos, Alexandra S Solovyova, Eefjan Breukink, Sven van Teeffelen, Mikhail M Savitski, Tanneke den Blaauwen, Athanasios Typas, and Waldemar Vollmer. Outer membrane lipoprotein NlpI scaffolds peptidoglycan hydrolases within multi-enzyme complexes in Escherichia coli. *The EMBO Journal*, 39(5):e102246, March 2020. Publisher: John Wiley & Sons, Ltd.

[4] Paola Bardetti, Felix Barber, and Enrique R. Rojas. Non-linear stress-softening of the bacterial cell wall confers cell shape homeostasis. *bioRxiv*, page 2024.09.03.611099, September 2024.

[5] David Hendricks Bergey. *Bergey's manual of determinative bacteriology*. Lippincott Williams & Wilkins, 1994.

[6] Gabriel Billings, Nikolay Ouzounov, Tristan Ursell, Samantha M. Desmarais, Joshua Shaevitz, Zemer Gitai, and Kerwyn Casey Huang. De novo morphogenesis in L-forms via geometric control of cell growth. *Molecular Microbiology*, 93(5):883–896, 2014. _eprint: https://onlinelibrary.wiley.com/doi/pdf/10.1111/mmi.12703.

[7] A. Boulbitch, B. Quinn, and D. Pink. Elasticity of the Rod-Shaped Gram-Negative Eubacteria. *Phys. Rev. Lett.*, 85(24):5246–5249, December 2000. Publisher: American Physical Society.

[8] Hongbaek Cho, Carl N Wivagg, Mrinal Kapoor, Zachary Barry, Patricia DA Rohs, Hyunsuk Suh, Jarrod A Marto, Ethan C Garner, and Thomas G Bernhardt. Bacterial cell wall biogenesis is mediated by seds and pbp polymerase families functioning semi-autonomously. *Nature microbiology*, 1(10):1–8, 2016.

[9] Yi Deng, Mingzhai Sun, and Joshua W. Shaevitz. Direct Measurement of Cell Wall Stress Stiffening and Turgor Pressure in Live Bacterial Cells. *Phys. Rev. Lett.*, 107(15):158101, October 2011. Publisher: American Physical Society.

[10] Michael F. Dion, Mrinal Kapoor, Yingjie Sun, Sean Wilson, Joel Ryan, Antoine Vigouroux, Sven van Teeffelen, Rudolf Oldenbourg, and Ethan C. Garner. Bacillus subtilis cell diameter is determined by the opposing actions of two distinct cell wall synthetic systems. *Nat Microbiol*, 4(8):1294–1305, August 2019. Publisher: Nature Publishing Group.

[11] Michael E. Fisher and Anatoly B. Kolomeisky. The force exerted by a molecular motor. *Proc. Natl. Acad. Sci. U.S.A.*, 96(12):6597–6602, June 1999.

[12] Leon Furchtgott, Ned S. Wingreen, and Kerwyn Casey Huang. Mechanisms for maintaining cell shape in rod-shaped Gram-negative bacteria. *Mol Microbiol*, 81(2):340–353, July 2011.

[13] Shambhavi Garde, Pavan Kumar Chodisetti, and Manjula Reddy. Peptidoglycan: Structure, Synthesis, and Regulation. *EcoSal Plus*, 9(2):eESP–0010–2020, 2021.

[14] B Glauner, J V Höltje, and U Schwarz. The composition of the murein of Escherichia coli. *Journal of Biological Chemistry*, 263(21):10088–10095, July 1988.

[15] James C. Gumbart, Morgan Beeby, Grant J. Jensen, and Benoît Roux. Escherichia coli peptidoglycan structure and mechanics as predicted by atomic-scale simulations. *PLoS Comput Biol*, 10(2):e1003475, February 2014.

[16] Kerwyn Casey Huang, Ranjan Mukhopadhyay, Bingni Wen, Zemer Gitai, and Ned S. Wingreen. Cell shape and cell-wall organization in Gram-negative bacteria. *Proc Natl Acad Sci U S A*, 105(49):19282–19287, December 2008.

[17] Saman Hussain, Carl N Wivagg, Piotr Szwedziak, Felix Wong, Kaitlin Schaefer, Thierry Izoré, Lars D Renner, Matthew J Holmes, Yingjie Sun, Alexandre W Bisson-Filho, Suzanne Walker, Ariel Amir, Jan Löwe, and Ethan C Garner. MreB filaments align along greatest principal membrane curvature to orient cell wall synthesis. *eLife*, 7:e32471, February 2018. Publisher: eLife Sciences Publications, Ltd.

[18] Joachim-Volker Höltje. Growth of the Stress-Bearing and Shape-Maintaining Murein Sacculus of Escherichia coli. *Microbiology and Molecular Biology Reviews*, 62(1):181–203, March 1998. Publisher: American Society for Microbiology.

[19] Robert M. Jones. *Mechanics of composite materials*. Taylor & Francis, Philadelphia, PA, 2nd ed edition, 1999.

[20] Tanvi Kale, Ryth Dasgupta, Mandar M. Inamdar, and Chaitanya A. Athale. Mechanics of E. coli cell width homeostasis and bulging dynamics from MreB

and septum inhibition, November 2024. Pages: 2024.11.22.624946 Section: New Results.

[21] Yuki Kitahara and Sven van Teeffelen. Bacterial growth—from physical principles to autolysins. *Current Opinion in Microbiology*, 74:102326, 2023.

[22] AL Koch. Additional arguments for the key role of "smart" autolysins in the enlargement of the wall of gram-negative bacteria. *Research in Microbiology*, 141(5):529–541, 1990.

[23] David T. Kysela, Amelia M. Randich, Paul D. Caccamo, and Yves V. Brun. Diversity Takes Shape: Understanding the Mechanistic and Adaptive Basis of Bacterial Morphology. *PLOS Biology*, 14(10):e1002565, October 2016. Publisher: Public Library of Science.

[24] MATLAB. *version R2024b*. The MathWorks Inc., Natick, Massachusetts, 2024.

[25] Paula P. Navarro, Andrea Vettiger, Virly Y. Ananda, Paula Montero Llopis, Christoph Allolio, Thomas G. Bernhardt, and Luke H. Chao. Cell wall synthesis and remodelling dynamics determine division site architecture and cell shape in Escherichia coli. *Nat Microbiol*, 7(10):1621–1634, October 2022. Publisher: Nature Publishing Group.

[26] Lam T. Nguyen, James C. Gumbart, Morgan Beeby, and Grant J. Jensen. Coarse-grained simulations of bacterial cell wall growth reveal that local coordination alone can be sufficient to maintain rod shape. *Proc Natl Acad Sci U S A*, 112(28):E3689–3698, July 2015.

[27] Enno R. Oldewurtel, Yuki Kitahara, and Sven van Teeffelen. Robust surface-to-mass coupling and turgor-dependent cell width determine bacterial dry-mass density. *Proc Natl Acad Sci U S A*, 118(32):e2021416118, August 2021.

[28] Patricia DA Rohs and Thomas G Bernhardt. Growth and division of the peptidoglycan matrix. *Annual review of microbiology*, 75(1):315–336, 2021.

[29] Enrique Rojas, Julie A. Theriot, and Kerwyn Casey Huang. Response of Escherichia coli growth rate to osmotic shock. *Proceedings of the National Academy of Sciences*, 111(21):7807–7812, May 2014. Publisher: Proceedings of the National Academy of Sciences.

[30] Johannes Schindelin, Ignacio Arganda-Carreras, Erwin Frise, Verena Kaynig, Mark Longair, Tobias Pietzsch, Stephan Preibisch, Curtis Rueden, Stephan Saalfeld, Benjamin Schmid, et al. Fiji: an open-source platform for biological-image analysis. *Nature methods*, 9(7):676–682, 2012.

[31] Jung-Ho Shin, Alan G Sulpizio, Aaron Kelley, Laura Alvarez, Shannon G Murphy, Lixin Fan, Felipe Cava, Yuxin Mao, Mark A Saper, and Tobias Dörr. Structural basis of peptidoglycan endopeptidase regulation. *Proceedings of the National Academy of Sciences*, 117(21):11692–11702, 2020.

[32] Alexander Stukowski. Visualization and analysis of atomistic simulation data with OVITO-the Open Visualization Tool. *MODELLING AND SIMULATION IN MATERIALS SCIENCE AND ENGINEERING*, 18(1), JAN 2010.

[33] Sean X. Sun and Hongyuan Jiang. Physics of Bacterial Morphogenesis. *Microbiology and Molecular Biology Reviews*, 75(4):543–565, November 2011. Publisher: American Society for Microbiology.

[34] Carolina Tropini, Timothy K. Lee, Jen Hsin, Samantha M. Desmarais, Tristan Ursell, Russell D. Monds, and Kerwyn Casey Huang. Principles of Bacterial Cell-Size Determination Revealed by Cell-Wall Synthesis Perturbations. *Cell Reports*, 9(4):1520–1527, November 2014.

[35] Robert D. Turner, Alexander F. Hurd, Ashley Cadby, Jamie K. Hobbs, and Simon J. Foster. Cell wall elongation mode in Gram-negative bacteria is determined by peptidoglycan architecture. *Nat Commun*, 4:1496, February 2013.

[36] Robert D. Turner, Stéphane Mesnage, Jamie K. Hobbs, and Simon J. Foster. Molecular imaging of glycan chains couples cell-wall polysaccharide architecture to bacterial cell morphology. *Nat Commun*, 9(1):1263, March 2018. Publisher: Nature Publishing Group.

[37] Tristan Ursell, Timothy K Lee, Daisuke Shiomi, Handuo Shi, Carolina Tropini, Russell D Monds, Alexandre Colavin, Gabriel Billings, Ilina Bhaya-Grossman, Michael Broxton, et al. Rapid, precise quantification of bacterial cellular dimensions across a genomic-scale knockout library. *BMC biology*, 15:1–15, 2017.

[38] Tristan S. Ursell, Jeffrey Nguyen, Russell D. Monds, Alexandre Colavin, Gabriel Billings, Nikolay Ouzounov, Zemer Gitai, Joshua W. Shaevitz, and Kerwyn Casey Huang. Rod-like bacterial shape is maintained by feedback between cell curvature and cytoskeletal localization. *Proc Natl Acad Sci U S A*, 111(11):E1025–1034, March 2014.

[39] Sven van Teeffelen and Lars D. Renner. Recent advances in understanding how rod-like bacteria stably maintain their cell shapes. *F1000Res*, 7:241, 2018.

[40] Sven van Teeffelen, Siyuan Wang, Leon Furchtgott, Kerwyn Casey Huang, Ned S. Wingreen, Joshua W. Shaevitz, and Zemer Gitai. The bacterial actin MreB rotates, and rotation depends on cell-wall assembly. *Proc Natl Acad Sci U S A*, 108(38):15822–15827, September 2011.

[41] Antoine Vigouroux, Baptiste Cordier, Andrey Aristov, Laura Alvarez, Gizem Özbaykal, Thibault Chaze, Enno Rainer Oldewurtel, Mariette Matondo, Felipe Cava, David Bikard, and Sven van Teeffelen. Class-A penicillin binding proteins do not contribute to cell shape but repair cell-wall defects. *eLife*, 9:e51998, January 2020. Publisher: eLife Sciences Publications, Ltd.

[42] Henri Voedts, Delphine Dorchêne, Adam Lodge, Waldemar Vollmer, Michel Arthur, and Jean-Emmanuel Hugonnet. Role of endopeptidases in peptidoglycan synthesis mediated by alternative cross-linking enzymes in Escherichia coli.

The EMBO Journal, 40(19):e108126, October 2021. Publisher: John Wiley & Sons, Ltd.

[43] Waldemar Vollmer and Joachim-Volker Höltje. The Architecture of the Murein (Peptidoglycan) in Gram-Negative Bacteria: Vertical Scaffold or Horizontal Layer(s)? *J Bacteriol*, 186(18):5978–5987, September 2004.

[44] Waldemar Vollmer, Bernard Joris, Paulette Charlier, and Simon Foster. Bacterial peptidoglycan (murein) hydrolases. *FEMS Microbiology Reviews*, 32(2):259–286, March 2008.

[45] X. Yao, M. Jericho, D. Pink, and T. Beveridge. Thickness and elasticity of gram-negative murein sacculi measured by atomic force microscopy. *J Bacteriol*, 181(22):6865–6875, November 1999.

[46] Kevin D. Young. Bacterial Shape: Two-Dimensional Questions and Possibilities. *Annu Rev Microbiol*, 64:223–240, 2010.

Appendix A

Appendix

A.1 Parameter table

The following this the parameter table used for most simulations, unless otherwise specified. Most values of physical parameters are taken from Nguyen et al's work.

A.2 Explanation of important algorithms

The following are brief summaries of some of the more important algorithms used in the simulations. The purpose of giving them in this form is to aid anyone trying to use the code to understand the logic for each function.

`cutRandom_peptide`

This function randomly selects and cuts an existing peptide bond from the simulation. It repeatedly chooses a random index in the list of peptide bonds (`PepbondList`) until it finds a bond that is not a glycan bond (i.e., its type is not 1). Once a valid bond is found, it is removed from the bond list and from the corresponding entries in the bond dictionary for both involved particles. The bond arrays are updated by calling the helper function, and simulation pointers are updated along with a counter (`p.rpc`) that tracks the number of peptide bond cuts.

`cutRandom_glycan`

This function is the same as `cutRandom_peptide`, but instead of sampling random bonds from the the list of peptides, it does so from the list of glycan bonds: `PGbondList`.

`getStrains`

This calculates the strain in the simulation box dimensions. It takes the initial dimensions ($Lx-0$, $Ly-0$) and the current dimensions (Lx, Ly), and computes the

Parameter	Description	Value
	PG physics	
k_g	Stiffness of glycan strands	11140 pN/nm
k_b	Bending energy of a glycan strand	250.8 pN nm
l_g	Relaxed length of a glycan disaccharide	1.0 nm
l_p (x_0)	Relaxed length of a peptide bond	1.0 nm
l_c	Contour length of the peptide bond	3.8 nm
k_{WLC}	Force constant for the worm-like-chain equation for peptides	15 pN/nm
P	Internal turgor pressure	Range
	Integration parameters	
`dt`	Time-step for integration	0.001
μ	Friction coefficient during position update	0.01
α	Friction coefficient for boundary box update	0.001
`max_box_step`	The maximum step size of the boundary box	0.001 nm
`max_node_step`	The maximum step size for each node	0.01 nm
`stop_thresh`	Fraction change of bond-lengths to determine equilibrium	0.0005
	Remodelling parameters	
`d`	Search radius for making a peptide cross-link	3 nm
`q`	Minimum space between glycan strands when multiple are being inserted simultaneously	5 nm
`f`	Minimum hole diameter filter during repair function - ignores holes smaller than this	3.5 nm
`pcp`	Peptide cutting percentage cuts pcp% of all peptides randomly	Range
`gcp`	Glycan cutting percentage cuts gcp% of all glycans randomly	Range
`cl_min`	Minimum percent of peptide cross-links on each side of a newly inserted glycan strand	Range
`cl_max`	Maximum percent of peptide cross-links on each side of a newly inserted glycan strand	Range

Table A.1: Parameters used for the 2DPG simulations, unless otherwise mentioned. The physical properties are taken from Nguyen et al's MD simulations [26]. It is worth noting that their paper treated glycan strands as a tetrasaccharide, while we treat it as a disaccharide. Accordingly, the parameters are changed accordingly.There is a typo in Nguyen et al's paper where they report $l_c = 4.8$nm. However, after looking at their code and also speaking to the author, we confirm that it should be 3.8nm. Integration parameters and remodelling parameters are emperically determined from simulations.

fractional change in the x and y directions as $(Lx - Lx - 0)/Lx - 0$ and $(Ly - Ly - 0)/Ly - 0$, respectively. The initial dimensions are the dimensions of the simulation box when the first equilibrium condition of the simulations are reached. If other simulations are being continued, then the equilibrium positions are read from the recall file.

`write_metadata`

This writes the simulation metadata to a text file.

`run_stats`

This function writes summary statistics of the simulation into a text file named "run-stats.txt" within the output folder. It records whether the simulation was completed, the number of insertion events executed, and the overall duration. This file serves as a summary of the simulation's performance, and is important to know if a run stopped short.

`lammps-datafile`

This is an important function that facilitates easy visualisation of the simulation. It writes a LAMMPS–formatted data file for a specific simulation timestep, allowing visualization of the simulation in software such as OVITO [32].

`cut_infinite_strand`

This function detects and cuts infinite strands or loops in the PG network. It uses a depth–first search (DFS) on the graph defined by the glycan bonds to detect cycles. As it goes deeper in the network, it keeps track of visited nodes and identifies loops when a node is encountered twice. When a loop is detected, one of the bonds in the cycle is removed to break the loop. The function returns a boolean flag indicating whether a loop was found and cut.

`multi_SynCut`

A complex function that implements a simultaneous synthesis and cutting (SynCut) procedure for adding new glycan strands. Depending on the simulation options (whether a single or multiple insertion is specified), it determines how many new strands to add as a function of the length of the system in x:

$$\text{Number of glycan additions} = \text{floor}(L_x / L_x^{eq})$$

where L_x is the current length of the system, and L_x^{eq} was the length after the first equilibration. For each new strand, the function first finds a valid x–position that is at least a specified distance (q nm) away from existing new strand positions. It then assigns y–positions with a small random offset to avoid perfect regularity. A temporary copy of the bond dictionary is made, and directional tags (e.g., left,

up, right, down) are assigned to new strand nodes to indicate the direction of the peptide stems. For each node of the new strand, the function then searches for nearby nodes from the pg network that can form new peptide bonds with the new strand based its distance from the node. If a node from the pg network is less than `d` nm from the node on the new strand, and also it is *not* already connected to another node via a peptide bond (i.e. it is free to bond), then this list is appended onto the list of neighbours for that new-strand node (`strand_neighbors`. Then, from the shuffled list of `strand_neighbors`, particles are sampled and based on the cosine similarity between a preferred direction and the actual displacement vector, the bond is made:

$$\mathbb{P}(\text{bond formation}) = \texttt{max}(0, \cos^3(\theta))$$

where θ is the angle between the new node's peptide stem and the node from the PG network. Once a bond pair is made, the loop over neighbor nodes is broken, and the function moves on to the next node on the newly inserted strand. Once all the nodes on the strand have been matched with a neighbor, bonds are randomly chosen, until as many as `cl_max` bonds are made on each side of the strand. If the newly formed bonds meet the requirements of having the correct number of cross-links: at least `cl_min` and at most `cl_max` on each side of the strand, the new strand is accepted; otherwise, a new random x location is chosen for the strand, and the process is retried up to 100 times. `cl_max` and `cl_min` are percentages of the expected number of peptide bonds from a perfectly ordered system. Finally, existing bonds (peptide and/or glycan) that cross the path of the new strand are cut, the global bond dictionary, particle positions, and simulation parameters are updated accordingly and simulation moves on.

`findHoles`

This function employs an image–processing approach to detect holes in the particle network. It converts particle positions into pixel coordinates on a grid based on a specified pixel density, creating a binary mask where particles are marked. The mask is then dilated using a circular kernel, which helps to fill in gaps and highlight regions with missing particles. The dilated mask is returned for further analysis of holes in the structure.

`label-regions`

Performs connected–component labelling on a binary image (with holes appearing as objects after inverting the mask). To handle periodic boundary conditions, the image is padded using a wrap–around mode before labelling. After labelling the connected regions, the padding is removed and corrections are made along the boundaries to merge regions that are connected via periodicity. The function then adjusts the label numbers to remove any gaps and returns the labelled mask along with the total number of regions identified. The output of labelled holes (as different colours) for a representative system is shown in Figure A.1

Figure A.1: An example of pores identified in the 2DPG system, with periodic boundaries considered using tiling. All regions of the same colour have the same label. For each region, the particles that fall within that region are identified as the boundary particles for that region.

`dilate-regions`

As described previously, in `findHoles` function dilates each labeled region individually using a circular kernel whose radius is determined by the pixel density and a scaling factor. It processes each region from the labeled mask and stores the dilated version in a three–dimensional array (where each slice corresponds to one region). This allows further analysis on each region independently, and the function returns the collection of dilated regions.

`compute_particle_angles`

Calculates the angles of border particles relative to a given centroid $(c - x,\, c - y)$. For each border particle, the displacement vector (adjusted for periodic boundaries) is computed, and the angle is determined using the arctan2 function. The resulting angles are collected into a NumPy array, which is then used for sorting the border particles along the region's perimeter.

`compute_pbc_centroid`

The centroid of a set of border particles for a given region is calculated, while handling periodic boundary conditions. It first computes the mean position of the border particles and then orders them based on their angle relative to this mean. To avoid discontinuities due to periodicity, the particle coordinates are "unwrapped" relative to a reference point. A closed polygon is then constructed from the ordered positions, and its perimeter is interpolated to create a smooth contour. The centroid of this contour is calculated and corrected for periodic boundaries before being

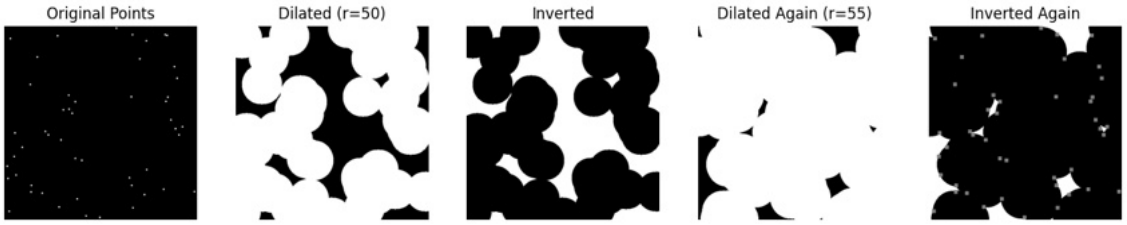

Figure A.2: **Step 1:** Put the nodes onto the image, and dilate them by r_1. **Step 2:** Invert the image to make the "holes" in white. **Step 3:** Filter out small holes, and then dilate these again by r_2. **Step 4:** The re-diluted holes will overlap with the boundary particles. Looking at which particles fall within the dilated hole, we identify the boundary nodes for that hole. Here, the points that are visible on a black background are boundary points. In this example, all holes are treated simultaneously and so it is not possible to say which particle is the boundary for which hole. However in the simulation, each hole is individually treated, and so the 'visible' boundary particles will only correspond to that hole.

returned.

`PGrepair`

This function repairs holes in the glycan network. It repeatedly performs the following steps up to a maximum number of iterations: converts particle positions to a pixel grid, creates a binary mask, inverts the mask, dilates the particle objects by radius r_1, and detects contours to identify holes as spaces left after the dilation. Small regions are filtered out, and connected components across boundaries are labelled with corrections for periodic boundaries. The image is then inverted again, and each labelled region is dilated by $r_2 = 1.1 \cdot r_1$, and border particles that lack peptide bonds are identified by looking at the nodes that fall within the newly dilated regions. The function then computes pairwise distances among these border particles to find candidate pairs that can be bridged by synthesizing a new glycan strand. If a suitable pair is found (based on a minimum separation, absence of existing bonds as well as a preference of being aligned to the shor-axis of the hole), a new strand is generated by interpolating positions and updating the bond dictionary. The simulation state (positions, bond arrays, counters, etc.) is updated, and the process is repeated if further repairs are needed. An example of the algorithm is illustrated in Figure A.2. If no candidate pairs are found, the hole is not fixed, and typically random cutting or insertion in that vicinity changes it so that the hole can be fixed.

`degrade`

This function cleans up the simulation by removing particles that have become isolated (i.e., those with one or fewer total bonds, counting both glycan and peptide bonds). It repeatedly identifies such particles, removes their bonds from both the bond dictionary and the global LAMMPS bond list, and sets their positions to

NaN to mark them as removed. This process continues until no particles meet the removal criteria, and then the simulation state (number of particles and bond arrays) is updated accordingly.

A.3 Notes on the evolution of the model

`SynCut`: simultaneous cutting and insertion

At first, insertion was implemented without cutting the underlying PG bonds. We imagined that the independent random cutting by the autolysins would eventually cut the underlying bonds, extend the cell in the x axis and bring the new strand under tension. However, we saw that these cuts were much rarer than we anticipated, and the added strands remained un-stressed for a long time. Additionally, the accumulation of 'limp' glycan strands resulted in the new peptide cross-links to "reach over" glycan strands and pull on neighbouring glycan strands too. This made the length of the cell was shrink, which is not physiological. While varying the search radius for the new peptides helped reduce how quickly the lengths shrunk, a search radius too small resulted in very few cross-links made. We also noticed that the recently inserted glycan strands began to serve as templates for the new strands, since they remained perfectly straight for a long time, and offered many new binding sites to the new straight glycan strand, such that they would start forming aggregates of long, parallel glycan strands.

To address these issues, we reduced the search radius to be small enough to reach neighbouring strands (typically $\approx$ 3nm away) and we incorporated the make-before-break rule, where the glycan and/or peptide bonds that cross the newly inserted glycan strands are cleaved immediately after the new cross-links are made. This caused the new glycan strands to immediately be incorporated into the network, thus causing the system length to increase, the "template" behaviour to break and also the glycan aggregates to stop forming. This change resulted in a drop of glycan densities, which actually resulted in a slower width decrease, but it is still preferred to artefactual glycan clumping. Figure A.3 shows how the cutting of the underlying bonds removes clumping.

`Repair`: including the role of aPBPs

In many of the initial simulations, cutting of glycans and peptides lead to very large pores forming in the system, often completely tearing the system. This prompted us to incorporate PG repair as a module. We simulated the role of aPBPs by algorithmically searching for large pores in the simulation based on the distances between nodes, and then filling those nodes with short glycan strands until no pores were left. For more details into the algorithm used to find and fill pores in the system, see chapter 2.

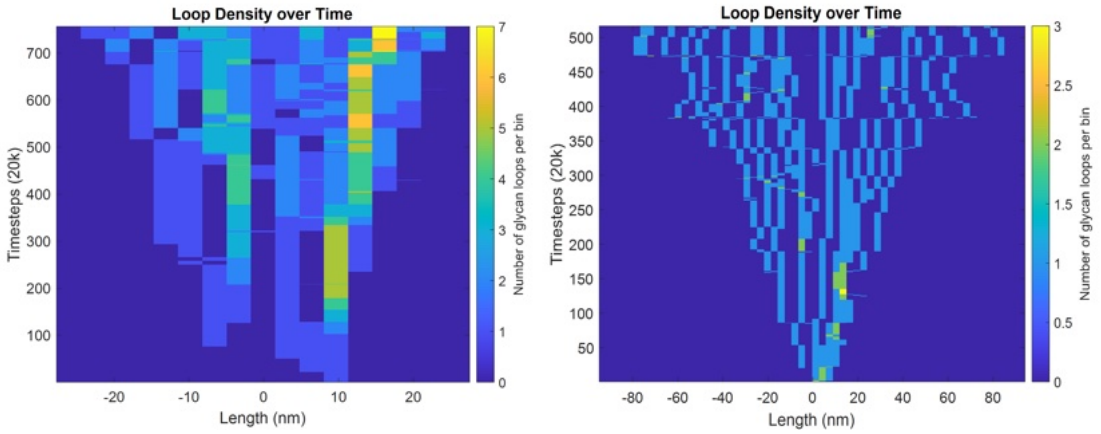

Figure A.3: Kymographs of glycan densities. Left: Glycan strands from large clumps when cutting of the underlying bonds is not implemented. Right: Glycan strands do not clump.

Custom module in C for fast equilibration

Simulating thousands of bonds over many insertions resulted in the simulation time increasing almost linearly with the number of bonds. While this was unavoidable, times of a few hours for only 10 insertions became very difficult to work with, especially in the testing phase when many parameters are being explored.

Initially, the program had been written fully in python. However, the timescales prompted us to port the equilibration steps into a custom parallelised module written in C, while leaving the insertion, repair and cutting algorithms in python for easy access. In the end, we achieved a 15-20x speed up, and a highly modular code with the system initialization and remodelling algorithms neatly arranged as easy-to-read and highly customizable python functions, and the parallelized equilibration code as an external module written in C. The simulations can be sped up even further using GPUs, however further optimisation was out of the scope of the project due to time constraints.

The modularity makes the 2DPG model an ideal platform for further development even by other researchers. For the code and a short guide on using it, please reach out to the van Teeffelen lab.

Periodic boundaries reduce minimum system size

Since it has been shown that the insertion of long glycan strands are important for width control, we needed a way to have very long glycan strands in the system, without making the whole system large and computationally infeasible. Following JC Gumbart's atomic scale model [15], we used periodic boundaries in both x and y directions, and were able to simulate "infinitely long glycan strands" by making long glycan strands loop around the whole system. This helped us maintain fast simulation times without having to give up on important mechanical properties of the PG layer.

A.4 Hyper-osmotic shocks lead to width increase

We saw in a pre-print by Enrique Rojas [4] that they have an experiment where they gave *Bacillus subtilis* cells a hyper-osmotic shock; thereby reducing the internal turgor pressure momentarily, and they saw that there was a reduction in width for a certain ΔOsm, but if the magnitude of the shock was increased, then the width started increasing again. This was interesting, as our simulations show that the modelled PG layer also has such a finger-trapping behaviour as described in chapter 2.2. So, we decided to repeat this experiment in order to understand how the magnitude of the effect may change with medium, strain or widths. It is worth noting that the osmotic shocks in Rojas' paper were in liquid culture, using microfluidics. As such, they had to use methods to bind the cells to the channels so that they don't flow away. The group had used the 'APTES' chip to mechanically sandwich the cells between the top and bottom surfaces, thus fixing them in place. We wondered if this could be affecting the results.

Additionally, older data from the van Teeffelen lab (by Yuki) using a different osmolyte (NaCl instead of the Sorbitol used by Rojas' lab) showed contrasting results, where no matter the magnitude of the shock, widths were always reduced.

To understand if the osmolyte or the cellasic chip caused this effect, we repeated the experiment in our lab using sorbitol, and on agar pads.

Method

Cell Culture: Wildtype B.subtilis PY79 cells were cultured in 3ml LB overnight at 30°C. In the morning, the OD_{600} was measured, and the culture was diluted to the OD of 0.0001. This culture was then incubated again at 30°C for about 10 generations, making sure that the OD never went beyond 0.3. After about 5 hours, and at an OD between 0.05 and 0.2, cells were imaged.

Sample preparation: 1%w/v UltraPure agarose pads were made with LB along with varying concentrations of Sorbitol, in 1mm thick moulds. They were left on the bench in their moulds for about 30 minutes, and then cut to 0.7 cm squares. $1\mu l$ of the sample was pipetted onto a circular glass (iBIDI) slide, and the pad was placed on top of the cells. Within 60 seconds of placing the pads, the cells were imaged using a custom imaging script for 5 minutes; where every image is an average of 5 snapshots. Only the first frame was considered for the analysis, as the effect of osmotic shifts are immediate, and we did not want to consider plastic changes in cell shape.

Result

Our results showed that like with NaCl, Sorbitol leads to a consistent width decrease for hyperosmotic shocks. Actually, the width strains were quite comparable with NaCl hyperosmotic shocks too (Figure A.4). This contradicts the pre-print in question, and we think the effect they see might be due to the confinement of the CellASIC chip, especially since the effect is seen near the same width as the

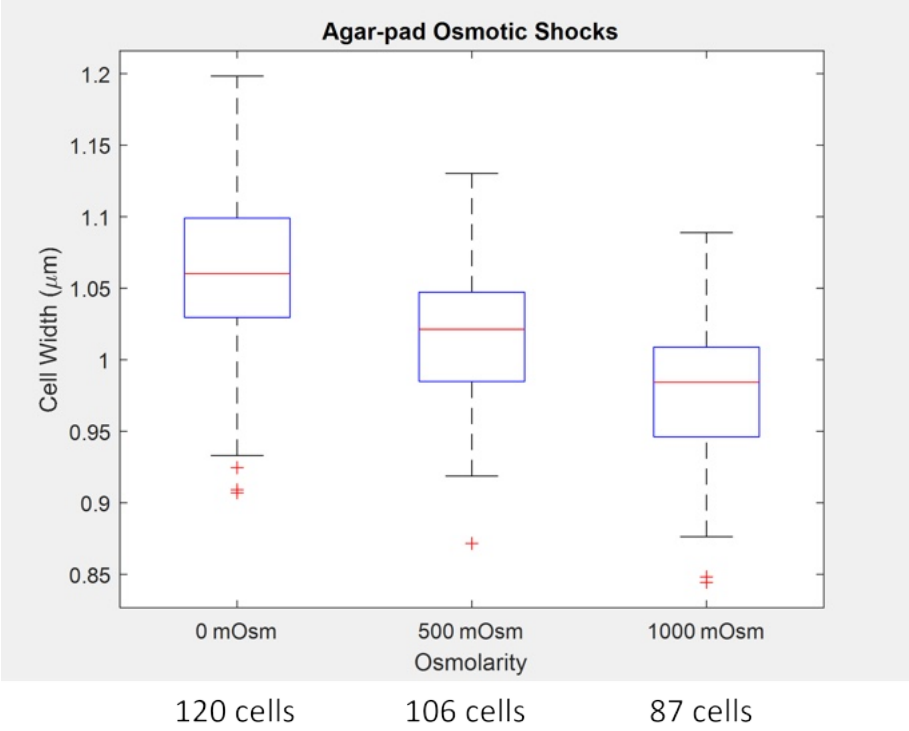

Figure A.4: Hyper-osmotic shocks of varying degree: Box plots of cell widths measured from snapshots immediately after osmotic shock using phase contrast microscopy, plotted as a function of the degree of osmotic shock. The numbers at the bottom correspond to the number of cells in the analysis.

CellASIC confinement. Thus, when compared to earlier data from the lab, we see that NaCl and Sorbitol induced osmotic shocks both cause width to increase by approximately the same amount.

A.5 Hyper-osmotic ramps

Osmotic shocks are sudden changes in the osmolarity of the growth medium in which bacteria are growing. This causes a sudden change in the osmotic pressure difference between the inside and the outside of the cells. Researchers often use such osmotic shocks to study the elastic effect of changes of turgor pressure in the cell [4] [29]. However, osmotic shocks have the caveat of being short-lived. Once pressures change, the cells begin osmo-adaptation to return their turgor pressure back to what it was [29] before the shock. This prevents the study of long-term effects of pressure changes. Osmotic ramp experiments attempt to circumvent this issue by continuously changing the external osmolarity of the medium, such that the cells do not have the time to 'catch up' to the pressure changes, and end up sustaining the changed turgor pressure for a longer time [27].

The changes in morphology that happen immediately after an osmotic shock are due to the elastic properties of the PG layer. This means they are generally reversible and are not brought about by explicit remodelling of the cell wall. We do such

experiments to understand the mechanical properties of the cell wall in section A.4. However, it is also interesting to see how a changed turgor pressure might affect the enzymatic remodelling of the cell to give rise to plastic changes in shape. In order to test this, we performed hyper-osmotic ramp experiments following the procedure in [27].

Method

Cell Culture: Wildtype E.coli MG1655 with SulA (S290) cells were cultured in 3ml LB overnight at 30°C. In the morning, the OD_{600} was measured, and the culture was diluted to the OD of 0.0001. This culture was then incubated again at 30°C for about 10 generations, making sure that the OD never went beyond 0.3. After about 5 hours, and at an OD between 0.05 and 0.2, cells were imaged.

Sample preparation: 1%w/v UltraPure agarose pads were made with LB along with 1mM IPTG to induce filamentation, in 1mm thick moulds. Another set of 3mm thick moulds were made, with 700mOsm NaCl. They were left on the bench in their molds for about 30 minutes, and then cut to 1 cm squares. 1ul of the sample was pipetted onto a ibidi slide, and the pad was placed on top of the cells. The cells were imaged using a custom imaging script for 5-10 minutes, and then the second 3mm thick pad was added on top of the 1mm pad on the microscope carefully to avoid any shifting, and the microscope was re-kohlered and re-focused as soon as possible. Exposure was adjusted so that the histogram peaked at around 30,000 (units). Cells were then imaged for an hour.

For control, the same as above was done, without NaCl in the second pad.

Result

Unexpectedly, the control showed a sudden increase in width by 5%. To test whether this was an effect of IPGT induced SulA, we tried adding the SulA in the culture, and waiting for 30 minutes to take effect. Even then, we saw an increase in the cell width over the course of a generation. Possibly, the addition of the pad caused the cells to have an un-intended hypo-osmotic shock. On close inspection of the control experiments performed earlier in the lab [27] we saw that this was a general trend. However, during a hypersmotic ramp, when NaCl is added in the second pad, we see a decrease in width of about 5% over one doubling time (A.5), concurrent with the data in literature. We concluded that pressure has an effect on the enzymatic remodelling in some way, since we see a plastic change of width. More experiments are required to look into how exactly pressure relates to remodelling, for example, by stress-dependent cutting, or by affecting the cross-linking availability due to a constant search radius.

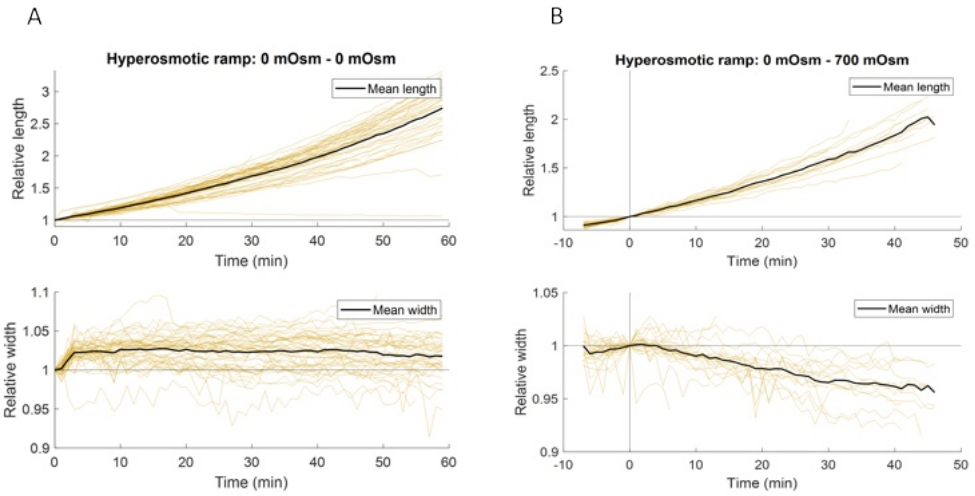

Figure A.5: Timelapse of cells in hyperosmotic ramp experiment: Lengths and widths of cells with 0 mOsm (A- control) and 700 mOsm (B- test) as a function of time in yellow, and the means plotted in black. The ramp in both cases is started at t=0min.

Appendix B

Supplementary figures

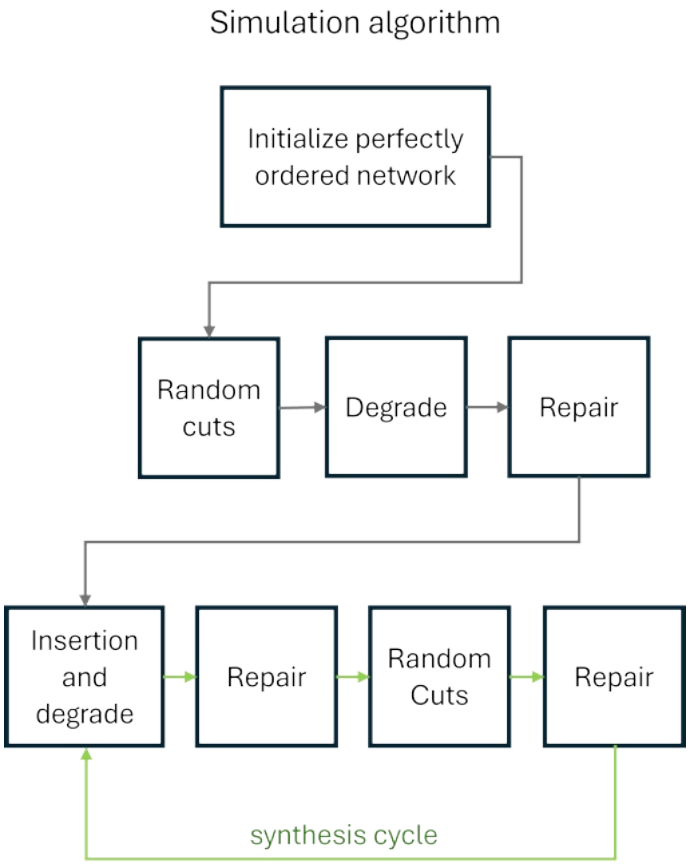

Figure B.1: Algorithm flowchart for most simulations: After the system is initialised, random cuts are made in order to introduce disorder at the beginning. Then, the deagrade and repair functions remove free-hanging bonds and fill holes respectively. After this, the patch enters the synthesis cycle, where rod-complex mediated synthesis, removal of lose bonds, random cuts, and repair happens in that order, loops until the simulation is stopped.

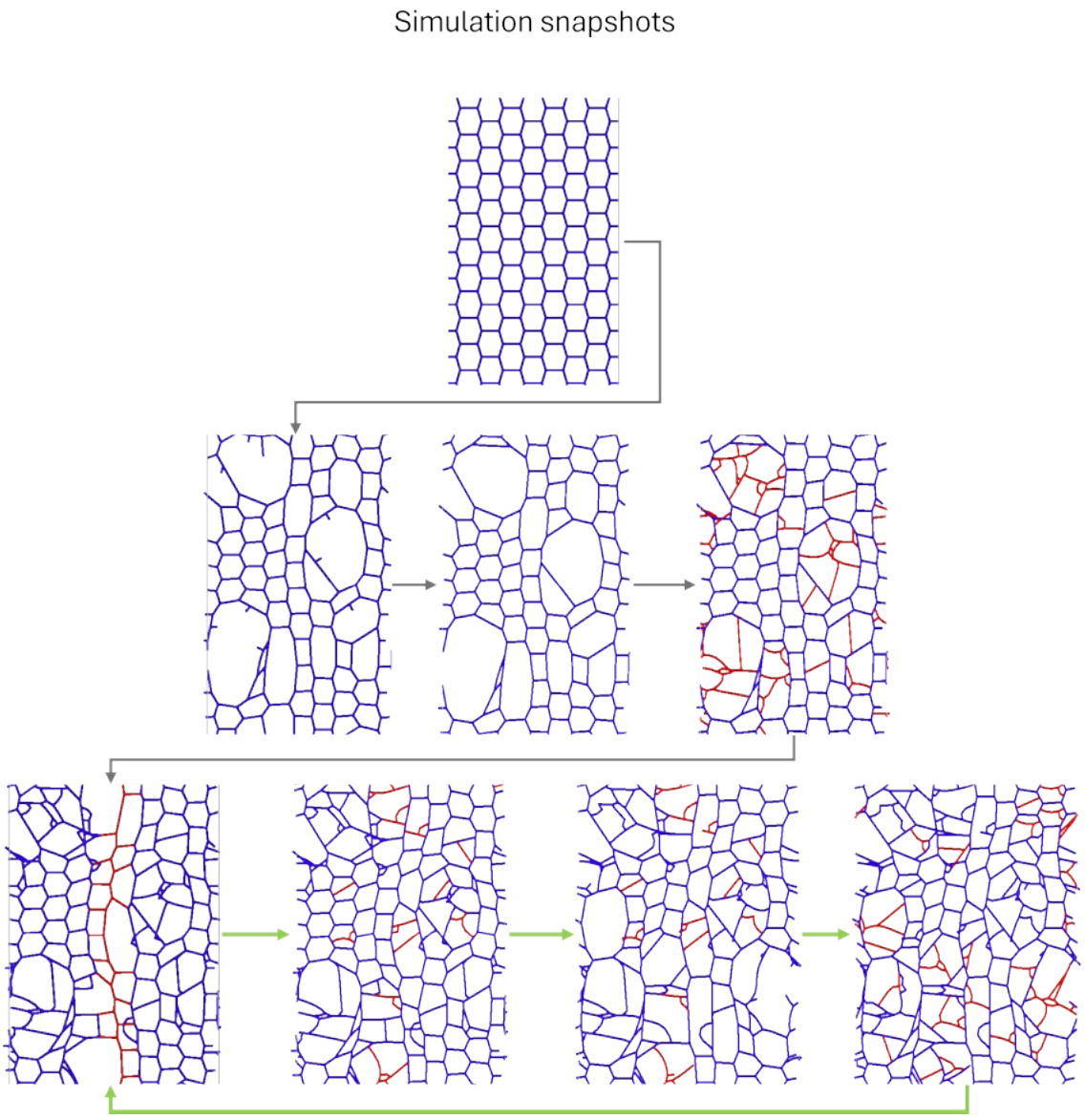

Figure B.2: Snapshots of the 2DPG layer at each step corresponding to the flowchart shown in Figure B.1. Here, the blue bonds are the old network bonds, and the red bonds correspond to the added material during each step.

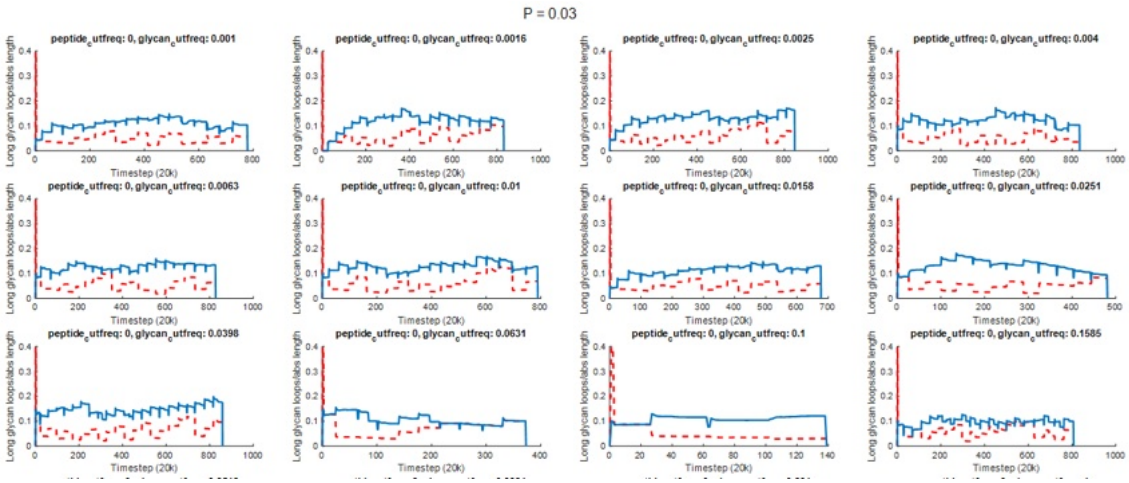

Figure B.3: Glycan densities are calculated by counting the number of infinite or looping glycans in the system at a given time and dividing by the system length at that time. Despite increasing glycan cutting frequencies, these simulations show that the glycan densities remain strikingly conserved close to 0.1 based on our insertion algorithms.

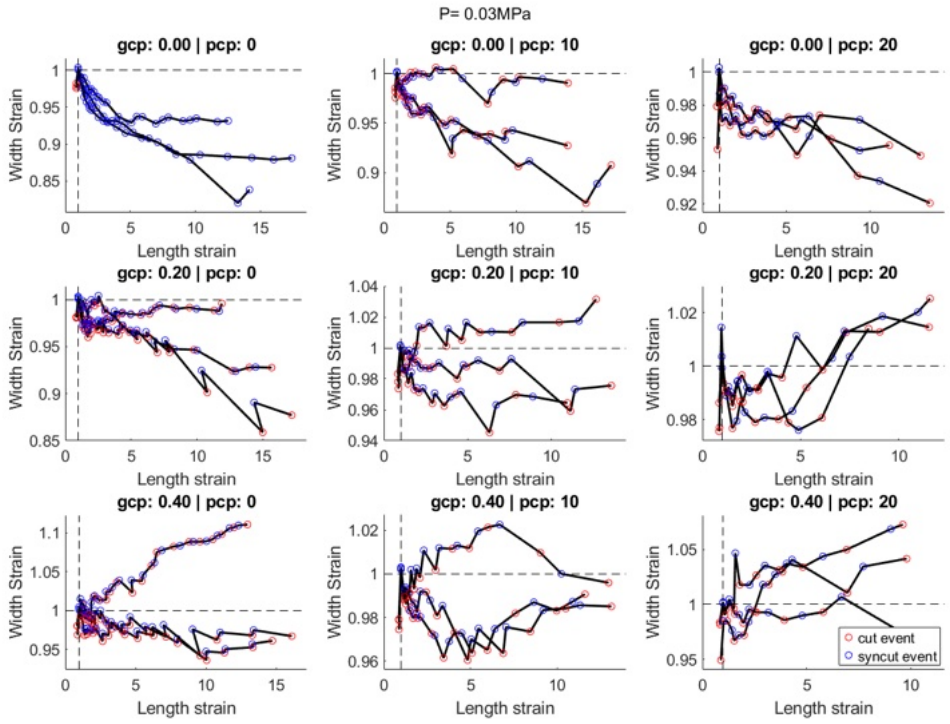

Figure B.4: Stochastic results: Multiple simulations over-layed shows the inherent stochasticity of the patch, while the trends discussed are still conserved.

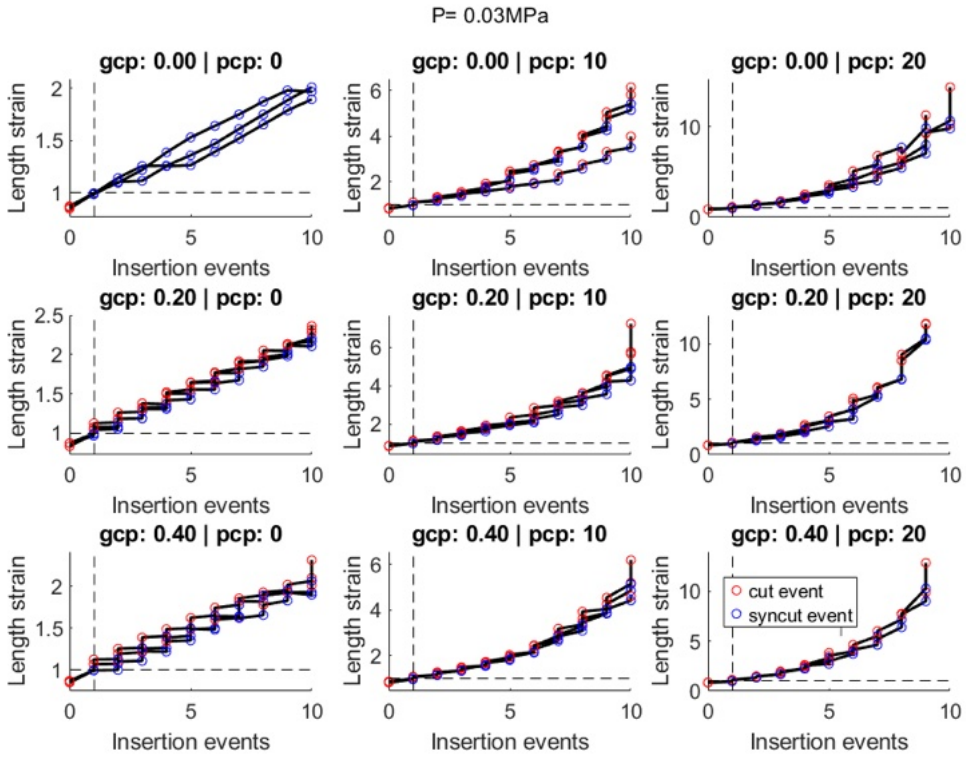

Figure B.5: Multiple simulation overlays of the same type of experiment as in Figure 3.6, but plotting length strains against number of insertions